Journal of the Geological Survey of Brazil

Geology and geochemistry of deformed granites from the Querari Complex, Rio Negro Province, NW-Amazonian Craton, Brazil

Paulo Jerry Bentes Gomes[1] (iD), Rielva Solimairy Campelo do Nascimento[1] (iD), Renata da Silva Veras[2*] (iD), Marcelo Esteves Almeida[3] (iD), Marcia Caroline Rodrigues Carneiro[4] (iD)

[1]Programa de Pós-Graduação em Geociências, Instituto de Ciências Exatas, Universidade Federal do Amazonas - UFAM, Av. General Rodrigo Octávio Jordão Ramos, 6200, Coroado, Manaus-AM, Brazil, CEP: 69080-900.
[2]Programa de Pós-Graduação em Geologia e Geoquímica, Instituto de Geociências, Universidade Federal do Pará - UFPA, Rua Augusto Corrêa,01, Guamá, Belém-PA, Brazil, CEP: 66075-110.
[3]Serviço Geológico do Brasil, Avenida Pasteur, 404, Urca, Rio de Janeiro - RJ, Brazil, CEP: 22290-255.
[4]Programa de Pós-Graduação em Geologia, Instituto de Geociências, Universidade de Brasília – UnB, Brasília - DF, Brazil, CEP: 70910-900.

Abstract

The Querari Complex corresponds to the basement rocks from Uaupés Domain and represents one of the least studied units in the northwest of the Rio Negro Province, Amazonian Craton. In this paper, we present new field geology, petrographic, and geochemical data of deformed granites from the Querari Complex. Based on our results, we suggest the differentiation of the Querari Complex into two magmatic facies. The Panã-Panã Facies comprises mainly porphyritic syeno to monzogranites with biotite as the main mafic mineral, and titanite, epidote, and allanite as accessory phases. The rocks of the Panã-Panã Facies have calc-alkaline and metaluminous affinities. The Matapi Facies has a syenogranite composition, coarse to porphyritic texture with magmatic muscovite and biotite, normative corundum higher than 1% (1.85-2.06), and mostly a peraluminous character. Both facies are generally enriched in silica and have a small spectrum of variation (67.5 to 70.1 wt.% Panã-Panã Facies - 71.1 to 73 wt.% Matapi Facies), but they differ by the high Al_2O_3, Fe_2O_3, MgO, CaO, Sr, and Ba contents in the Matapi Facies. Geological and geochemical compositions suggest that the magmatic precursors of these rocks of Matapi Facies may be derived from partial melting of metasedimentary sources, whereas the Panã-Panã Facies are probably derived from a meta-ignea source of intermediate composition, such as tonalitic gneisses. The rocks of the Querari Complex would have been generated in the collisional tectonic settings during the Paleoproterozoic (between 1778 and 1740 Ma). During this 1.78-1.74 Ga tectono-magmatic event (D_1), the magmatic fabric (S_0) and the parallel S_1 foliation have been developed, with NE-SE orientation. A subsequent tectonic event (D_2) was responsible for the folding S_1 foliation, creating the S_2 axial planar foliation with an approximate orientation E-W. This D_2 event is thought to represent a Calymmian (1.52 - 1.48 Ga) tectono-metamorphic event, associated with widespread I- and S-type granite emplacement in the Rio Negro Province. The deformation textures, as well as the mineral paragenesis for the Panã-Panã and Matapi facies, reveal temperature conditions at upper amphibolite facies, up to 700ºC. Finally, the D_3 tectono-metamorphic event comprises the reactivation of many NE-SW ductile shear zones with sinistral kinematic, creating a mylonitic foliation (S_3) in the rocks of the Querari Complex. This D_3 tectono-metamorphic event is probably linked to the intracratonic K´Mudku tectono-metamorphic event (between 1317 and 1198 Ma) of the Amazonian Greenvillian-Sunsás continental collision.

1. Introduction

Granitic rocks are one of the main components for geotectonic reconstruction studies, owing to their inherent feature of registering tectono-metamorphic events in a determined area, recorded by their structural and geochemical characteristics (e.g., Pitcher 1997, Janoušek et al. 2020). In the north-western region of Rio Negro Province, in the Amazonian Craton (Fig. 1a, 1b), several plutonic rocks have been reported in the literature, but studies are still scarcer because of the difficulty in accessing the area.

The Rio Negro Province has been initially subdivided into two tectono-stratigraphic domains: Imeri (east) and Alto Rio Negro (west) (Fig. 1b; Almeida 2006). More recently, based on

field, geochemical, and geochronological data from basement rocks and intrusive granitoids, Almeida et al. (2013) reviewed the previous domains and subdivided the Alto Rio Negro Domain into two new domains: the Içana and Uaupés domains (Fig. 1b). The Içana Domain comprises several migmatites, orthogneisses and metagranitoids with crystallization ages at ca. 1.81 Ga, and migmatization ages at ca. 1.79 Ga (Almeida et al. 2013, Veras et al. 2018). On the other hand, the Uaupés Domain comprises mainly orthogneisses and calc-alkaline metagranitoids with monzogranitic to dioritic composition with 1740 ± 2 Ma (Single-zircon Pb-evaporation), all included in the Querari Complex (Almeida et al. 2013).

In addition, there are several intrusive granitoid types in both Içana and Uaupés domains (Fig. 1b), including S-type granitoids dated at 1546 ± 11 Ma (Single-zircon Pb-evaporation; Almeida 2006), 1521 ± 32 Ma (Single-zircon Pb-evaporation; Almeida et al. 1997) and 1521 ± 13 Ma (U-Pb ID-TIMS in zircon; Tassinari et al. 1996); and I-type granite dated between 1518 ± 25 Ma (U-Pb ID TIMS in zircon; Santos et al. 2000), and 1483 ± 2 Ma (Single-zircon Pb-evaporation; Almeida et al. 2013). However, despite these available geochronological data, in our opinion, there is no clear geological contextualization for these data. The absence of systematic studies integrating these geochronological data with petrographic, structural and geochemical information makes it difficult to compare and/or correlate them with other domains of the Amazonian Craton. In this contribution, we aim to discuss the tectonic-metamorphic characterization of the Uaupés Domain, especially on the basis of our observations and samples collected from granitic rocks that outcrop along the Içana River at the Brazil – Colombia border. In this work, we present field and whole-rock geochemical data to discuss the petrogenesis and possible tectonic setting of the study granitic rocks. We also attempt to understand if their genesis is related to the same orogenic event (Cordani et al. 2016), or if they, alternatively, represent distinct evolutionary episodes (Almeida et al. 2013).

2. Regional Geology: Querari Complex and Intrusive Granitoids

Here we adopted the Querari Complex designation suggested by Almeida et al. (2013) for the basement rocks of the Uaupés Domain (Fig. 1b). The Querari Complex (Almeida et al. 2013) is composed of orthogneisses and metagranitoids with monzogranitic to granodioritic composition, constituted by feldspar, quartz, biotite, titanite, hornblende and eventually epidote, sulfide, and magnetite. These rocks have grayish color, are medium to coarse-grained, and have inequigranular to porphyritic texture with tabular K-feldspar phenocrystals up to 15 cm in size. Foliation is mainly defined by mafic mineral alignment and lenticular mafic enclave agglomerates trending from N30ºE to N10ºW. In addition, subparallel mylonitic foliation is commonly associated. The main foliation is often transposed by N70ºE to E-W trending shear zones.

Available geochronological data for the rocks along the Uaupés River (Brazil – Colombia border) are evidence that the Querari Complex has a crystallization age for the dominant protoliths of 1740 ± 2 Ma (single-zircon Pb-evaporation), with 1.82 Ga Nd model age (TDM) and εNd of +4.05 (Almeida et al. 2013). Younger dates for the crystallization age (1703± 7 Ma, zircon U-Pb ID TIMS; Tassinari et al. 1996) were found

in a quartz diorite also from the Uaupés River, and it was also interpreted as Querari Complex.

The structural-controlled granitoids bodies with NE-SW trend, sub-circular to elliptical shapes, and with high radiometric values (geophysical airborne data) in Uaupés Domain were correlated by Almeida (2006) with the Tiquié Intrusive Suite (oxidized A-type granites) described by Almeida (1997) in the Imeri Domain. Almeida et al. (2013) consider these granitoids as indiscriminate types. On the Colombian side, these granitoids are widely correlated with the Parguazan event (~1.5 Ga). Their composition goes from monzogranite to syenogranite, pink grayish color, equigranular to porphyritic texture constituted by microcline, micro-perthitic orthoclase, plagioclase, quartz, biotite, titanite, opaque minerals, hornblende, apatite, allanite, fluorite and zircon, and as secondary minerals, epidote, titanite and sericite (Almeida 2006). Geochemical studies on major elements (Almeida 1997) indicate sub-alkaline, metaluminous signature, similar to that of A2-type granites (Eby 1992). According to Almeida (2006), the SHRIMP U–Pb analyses of zircon and Single-zircon Pb-evaporation provided an age between 1749 ± 5 Ma and 1746 ± 5 Ma for crystallization, and an age of 2.03 Ga interpreted as inherited (1 zircon), showing a similar age to that of the Querari Complex.

3. Materials and methods

The methods adopted in this study consisted of systematic sampling during fieldwork, coupled with structural data taken from fourteen outcrops placed along the Içana River, Jauaretê Creek, and Caranguejo Mountain (Fig. 1c). Subsequently, petrographic and micro-structural studies were carried out on the oriented thin section.

Fourteen selected samples of the deformed granites from the Querari Complex were prepared for whole-rock chemical analyses. The preparation process included crushing, quartering, and grinding to the 200-mesh fraction) in the Lamination Laboratory of the Department of Geoscience at Universidade Federal do Amazonas. The analyses were performed at the ALS Brazil Laboratory. The samples were digested using lithium metaborate/tetraborate. Loss on ignition (LOI) was calculated after 1000ºC incineration. The analysis of the major elements was performed by Inductively Coupled Plasma Emission Spectrometry (ICP-AES), and trace elements (Y, Sr, Rb, Zr, Nb, La, Sr, Ce, Tb, Ba, Hf, Th, Ta, Nd, Tm, Sm, and REE) were determined by Inductively Coupled Plasma Mass Spectrometry (ICP-MS). The results of the lithochemical analyses were organized in a Microsoft Excel spreadsheet. For normative composition and geochemical classification, the GeoChemical Data toolkit 4.1 software (GCDkit; Janoušek et al. 2006) was used. Owing to their porphyritic texture, the classification of the rocks was based on normative composition.

4. Results

Two lithological groups were identified based on petrographic and geochemical data presented in this work. The previously identified lithologies in the area are correlated with the Querari Complex and indiscriminate granitoids rocks (Almeida 2006, Almeida et al. 2013). However, structural, microtextural, and petrographic data collected in this study show that all these rocks have a similar tectonic-metamorphic
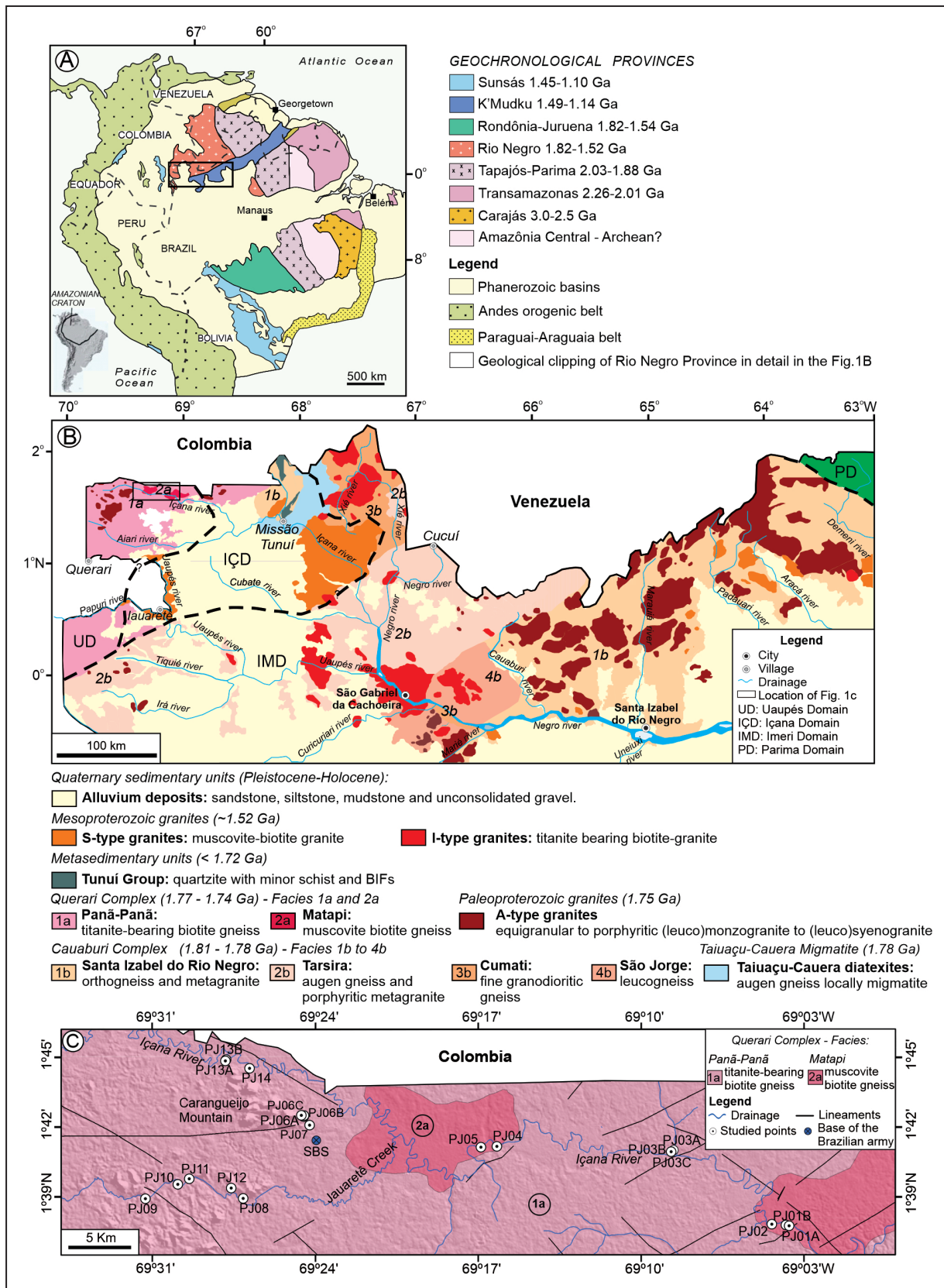
FIGURE 1. (a) Distribution of the Geochronological Provinces of the Amazonian Craton according to Santos et al. (2006); (b) Geological setting of the Rio Negro Province modified according to Almeida (2006). Limit of tectonic domains (dashed black line) according to Almeida et al. (2013). Addition of the Cauaburi Complex: São Jorge Facies (Carneiro et al. 2017), Cumati Facies (Almeida et al. 2013, Carneiro et al. 2017) and the Santa Izabel do Rio Negro Facies, which outcrop in the Içana Domain (Veras et al. 2015), and Taiuaçu-Cauera diatexite (Veras et al. 2018); (c) Simplified geological map of the study area, with the location of the study samples. SBS= Special Border Squad base of the Brazilian Army.

evolution and, therefore, may comprehend basement rocks of the Querari Complex. Thus, the deformed indiscriminate granitoid rocks are interpreted here as belonging to the Querari Complex. In addition, in this study, the Querari Complex has been subdivided into two distinct facies: the Panã-Panã and Matapi facies, named after the geographic area where they were found.

4.1. Field geology and petrography of the Querari Complex

The rocks of the Querari Complex mainly outcrop along the margins of the Içana River, Jauaretê Creek, and the Caranguejo Mountain. The latter is located near the border squad of the São Joaquim military base (Fig. 1c). Syeno to monzogranitic metagranites are the dominant lithologies of the Panã-Panã Facies, while in Matapi Facies, syenogranites and subordinate alkali feldspar granites are the dominant rock types (Fig. 2).

The **Panã-Panã Facies** comprises metagranites (Fig. 3a, 3b, 3c) that are equivalent to what was named as Querari Complex, according to previous literature (Almeida 2006, Almeida et al. 2013). These rocks present grayish to pinkish color, and inequigranular to porphyritic textures (Fig. 3b, 3a). Porphyroclasts are composed of microcline and plagioclase ($An_{8.9-29.6\%}$), and have tabular and stretched shapes, up to 5 cm in length (Fig. 3a). They are immersed in a medium-grained matrix composed essentially of quartz, K-feldspar, plagioclase ($An_{3.6-16.1\%}$), biotite, titanite, epidote, allanite, fluorite, zircon, and opaque minerals. The deformed granites are inequigranular to slightly porphyroblastic, and the main foliation is highlighted by biotite (Fig. 3c) and deformed porphyroclasts (Fig. 3b). In rocks with a higher percentage of porphyroclasts, metamorphic foliation development is incipient, preserving magmatic structures and orientation (Fig. 3a).

The rocks of the **Matapi** Facies have no equivalent units registered by previous literature, and their occurrences are much more restricted than those of the Panã-Panã Facies (Fig. 1c). They are metagranites with gray to pink color, with inequigranular to porphyritic textures (Fig. 3d, 3e, 3f). Microcline and subordinate plagioclase ($An_{10.1-18.7\%}$) represent the main porphyroclasts, with sizes ranging from 1 to 3 cm, and tabular (defining the orientation of magmatic flow; Fig. 3e) to sigmoidal shapes (when reworked in shear zones; Fig. 3f). The matrix of the rock is constituted by K-feldspar, plagioclase ($An_{6.6-12.5\%}$), quartz, biotite, and primary muscovite as essential minerals, and epidote, apatite, allanite, zircon, and opaque minerals as accessory minerals. At the PJ-05 outcrop (Fig. 1c), a 30 cm sized quartzite xenolith was found within a granite of the Matapi Facies (Fig. 3g).

In addition to the petrographic distinctions, both facies present the same deformational pattern and, therefore, all observed features in the Panã-Panã and Matapi facies will be described together here. In general, four foliations have been observed: (1) magmatic flow foliation (S_0) is characterized by tabular feldspar phenocrysts, with preferential orientation to NE-SW (Fig. 3a, 3e); (2) S_1 foliation oriented to NE (parallel to S_0 foliation) marked by biotite orientation (Fig. 3b, 3c, 4a), rotated feldspar porphyroblast orientation and mylonites (Fig. 3f, 4a, 5a); (3) S_2 foliation oriented to E-W (Fig. 4b), represents the axial plane of the asymmetric folded quartz veins and pegmatite dykes (Fig. 5b, 5c, 5d) installed along

the S_1 foliation (NE-SW); and (4) S_3 foliation observed only in thin sections (described in item 4.2.3), defined by minerals without deformation parallel to the deformed minerals of S_1 foliation.

4.2. Overprinting relationships of microstructures and inference of the development conditions of foliations

4.2.1. S_0 and S_1 foliations

Some parallelism can be observed between tabular feldspar phenocrystal orientation and deformational features in thin sections that were developed in solid-state and characterizes $S_0//S_1$ (Fig. 6a, 6b). The S_1 foliation is defined by feldspar porphyroclasts (Kf and Pl-S_1) and deformed magmatic titanites (Ttn-S_1) on **Panã-Panã Facies**, plus biotite, magmatic epidote, magnetite, and ilmenite (Fig. 6a, 6b, 6c). Titanite presents a sigmoidal shape with undulose extinction (Ttn-S_1; Fig. 6a, 6b) as an indicator for sinistral kinematics, as well as biotite. Plagioclase porphyroclasts display tabular and sometimes curved shapes; they are also fractured, altered to sericite, and often have recrystallized boundaries (Pl-S_1; Fig. 6a). Internally, they exhibit deformation twinning, undulose extinction, subgrain development, grain-boundary migration, and interlobate-type quartz grain boundaries (Kf-S_1; Fig. 6c). The S_1 foliation on **Matapi Facies** is represented by feldspar porphyroclasts, muscovite, and biotite that occurs isolated or as mafic agglomerates associated with epidote, allanite, magnetite, and ilmenite. Porphyroclasts of K-feldspar show flame-shaped perthites with undulose extinction that often creates subgrains. Porphyroclasts of plagioclase are
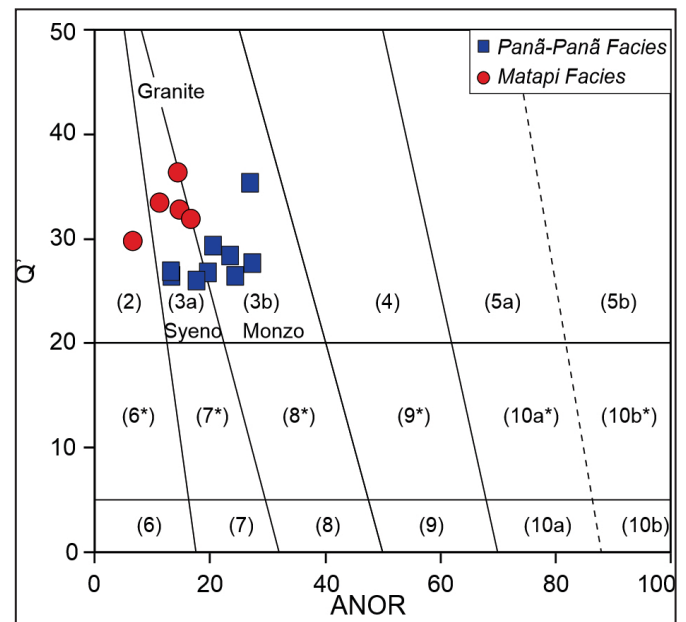
FIGURE 2. Classification diagram for Q'- ANOR plutonic rocks using their molecular normative compositions (according to Streckeisen and Le Maitre 1979), showing the granitic composition of the basement rocks of the Uaupés Domain. Q'= [Q/(Q+Or+Ab+An)]x100 and ANOR= 100xAn/(Or+An). Fields: (2) alkali-feldspar granite, (3a) syenogranite, (3b) monzogranite, (4) granodiorite, (5a) tonalite, (5b) calcic tonalite, (6*) alkali-feldspar quartz syenite, (7*) quartz syenite, (8*) quartz monzonite, (9*) quartz monzodiorite, (10a*) quartz diorite, (10b*) quartz gabbro, (6) alkali-feldspar syenite, (7) syenite, (8) monzonite, (9) monzogabbro, (10a) diorite, (10b) gabbro.
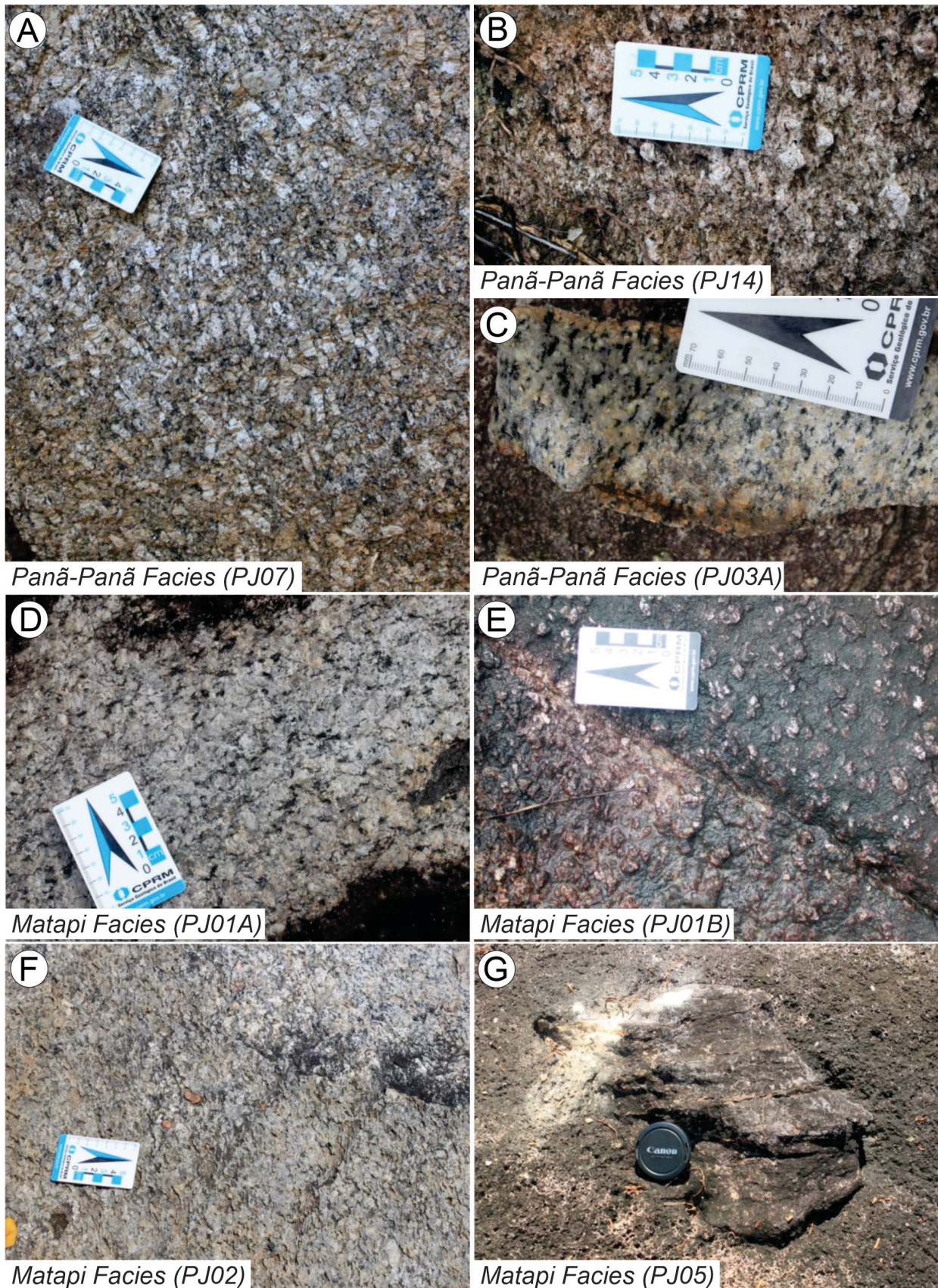
FIGURE 3. Mesoscopic aspects of deformed granites of the Querari Complex. (a) Metagranite of the Panã-Panã Facies with a well-defined fabric of K-feldspar megacrystals indicating magmatic foliation (PJ07); (b) Large lenticular eye-shaped feldspar representing the texture of an augen gneiss from the Panã-Panã Facies (PJ14); (c) Panã-Panã metagranite showing the well-developed mm-spaced banding marked by layers of mafic minerals (PJ03A); (d) The Matapi Facies showing coarse-grained to porphyroclastic with a slightly mineral orientation (PJ01A); (e) Metagranite of the Matapi Facies with feldspar phenocrystals (PJ01B); (f) Matapi metagranite showing the S_1 foliation associated with shear zones (PJ02); (g) Flattened and angular metasedimentary xenoliths hosted by metagranite of the Matapi Facies (PJ05).
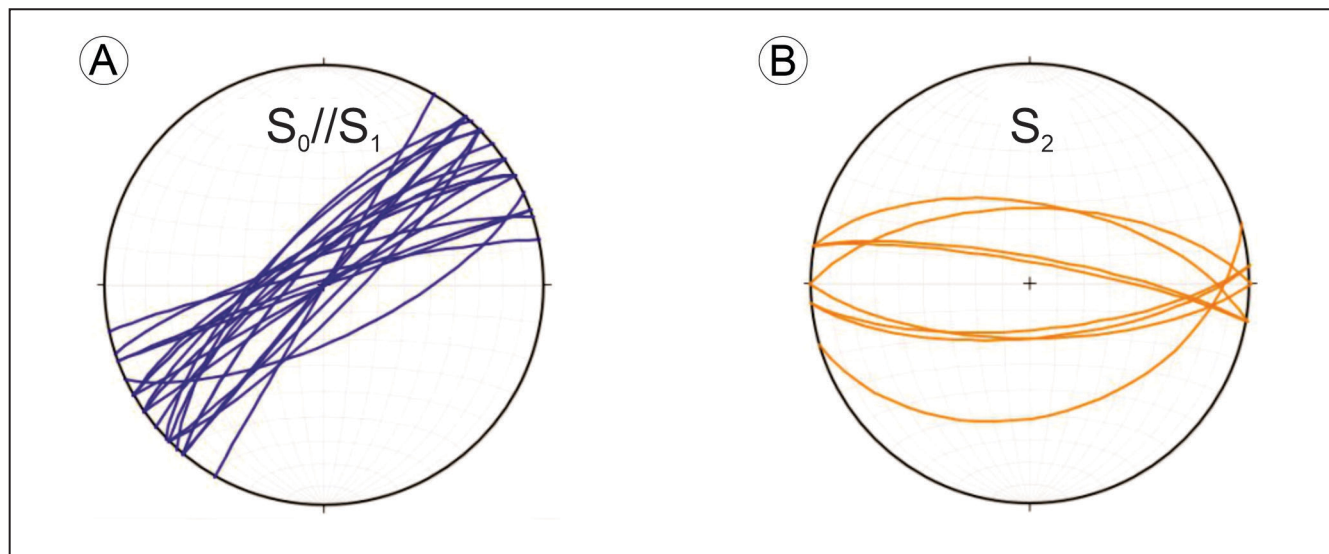
FIGURE 4. Stereographic projection of (a) S_0//S_1 foliations and (b) S_2 foliation of the Querari Complex.

scarce; also, they produce curved twinning and interlobate boundaries with quartz (Fig. 7a). Muscovite and biotite exhibit undulose extinction and show kink bands that commonly present crenulated cleavage (Fig. 7b).

4.2.2. S_2 foliation

The S_2 foliation is highlighted by the restricted development of titanite (Ttn- S_2; Fig. 6a) and deformed biotite (Bt- S_2; Fig. 6b) on **Panã-Panã Facies** which are oriented according to the axial plane of the folded S_1 foliation. Titanite (Ttn- S_2) displays a euhedral shape, corroded boundaries, opaque inclusions, and epidote (Fig. 6a). There are also small-sized elongated crystals according to the S_2 cleavage plane of biotite. On **Matapi Facies**, the S_2 biotite and S_2 muscovite occur on the axial plane of the folded S_1 foliation (Fig. 7b); furthermore, the deformation twinning of feldspar and plagioclase porphyroclasts (Pl- S_1) show lobate boundaries with quartz (Fig. 7a). The S_2 foliation that slightly crenulates the S_1 foliation found on the gneisses of Panã-Panã and Matapi facies is related to the deformational event and indicates upper amphibolite facies, in which temperature goes up to 700ºC. Textures such as deformation twinning of plagioclase and perthite occurrence express recrystallization process up to 650ºC (Yund and Tullis 1991), lobate boundaries between quartz and feldspar grains suggest temperature rates between 650ºC to 750ºC (Gower and Simpson 1992). Besides the microtextures listed above, there was a mineral association which characterizes an upper amphibolite facies paragenesis (e.g., titanite, magnetite, epidote, biotite, and plagioclase with anorthite content $An_{>17\%}$).

4.2.3. S_3 foliation

The S_3 foliation on **Panã-Panã Facies** is highlighted by euhedral titanite without deformation (Ttn-S_3; Fig. 6a), which points to some parallelism between S_3 and S_1 foliations. This foliation is also composed of biotite (Bt- S_3; Fig. 7d), epidote, magnetite, ilmenite, and porphyroblasts of K-feldspar (Kf-S_3; Fig. 6a, 7d) and plagioclase. Feldspar smaller crystals that

belong to the matrix of the rock show granoblastic texture, with no undulose extinction, indicating static recrystallization. Porphyroclasts of quartz present a chessboard-type subgrain texture and on the most deformed rocks, they occur as elongated ribbon aligned in S_3 foliation. The S_3 foliation on **Matapi Facies** is composed of biotite, muscovite, K-feldspar, plagioclase, and quartz. The K-feldspar occurs both as porphyroblasts (Kf- S_3; Fig. 7e) and as porphyroclast crystals that belong to the matrix of the rock (Fig. 7f). The latter are subhedral with preserved twinning and without deformation, as an indicator for static recrystallization. Quartz shows anhedral crystals, with interlobate to saw-tooth shaped boundaries, and exhibit subgrain and chessboard texture. Late euhedral titanite (Ttn- S_3), without deformation, parallel to S_1, associated with magnetite, epidote, biotite, and plagioclase ($An_{>17\%}$) characterize an upper amphibolite facies paragenesis. Subgrain and chessboard texture on quartz indicate recrystallization temperature around 680º to 700ºC (Kruhl 1996). Quartzo-feldspathic matrix granoblastic texture demonstrates recrystallization up to 650ºC (Yund and Tullis 1991). Lobate boundaries between quartz and feldspar grains suggest temperatures at around 650º and 750ºC (Gower and Simpson 1992). This event reached temperature enough to initiate the anatexis process, which is highlighted by plagioclase cuspate boundary with K-feldspar, drop-shaped quartz on feldspar besides the recrystallized K-feldspar occurrence.

4.3. Multielement geochemistry

A total of fourteen representative samples of deformed granites from Querari Complex were selected for whole-rock geochemical investigation (Table 1). The mineralogical differences between the Panã-Panã and Matapi facies are a consequence of the contents of the major and minor elements, along with the Rare Earth Elements (REE) patterns and High Field Strength Element (HFSE) abundances (e.g., Hf, Zr, Ti, Nb, and P) in these rocks.

Regarding major and minor elements, the samples of the Panã-Panã Facies differ from the Matapi Facies by slightly
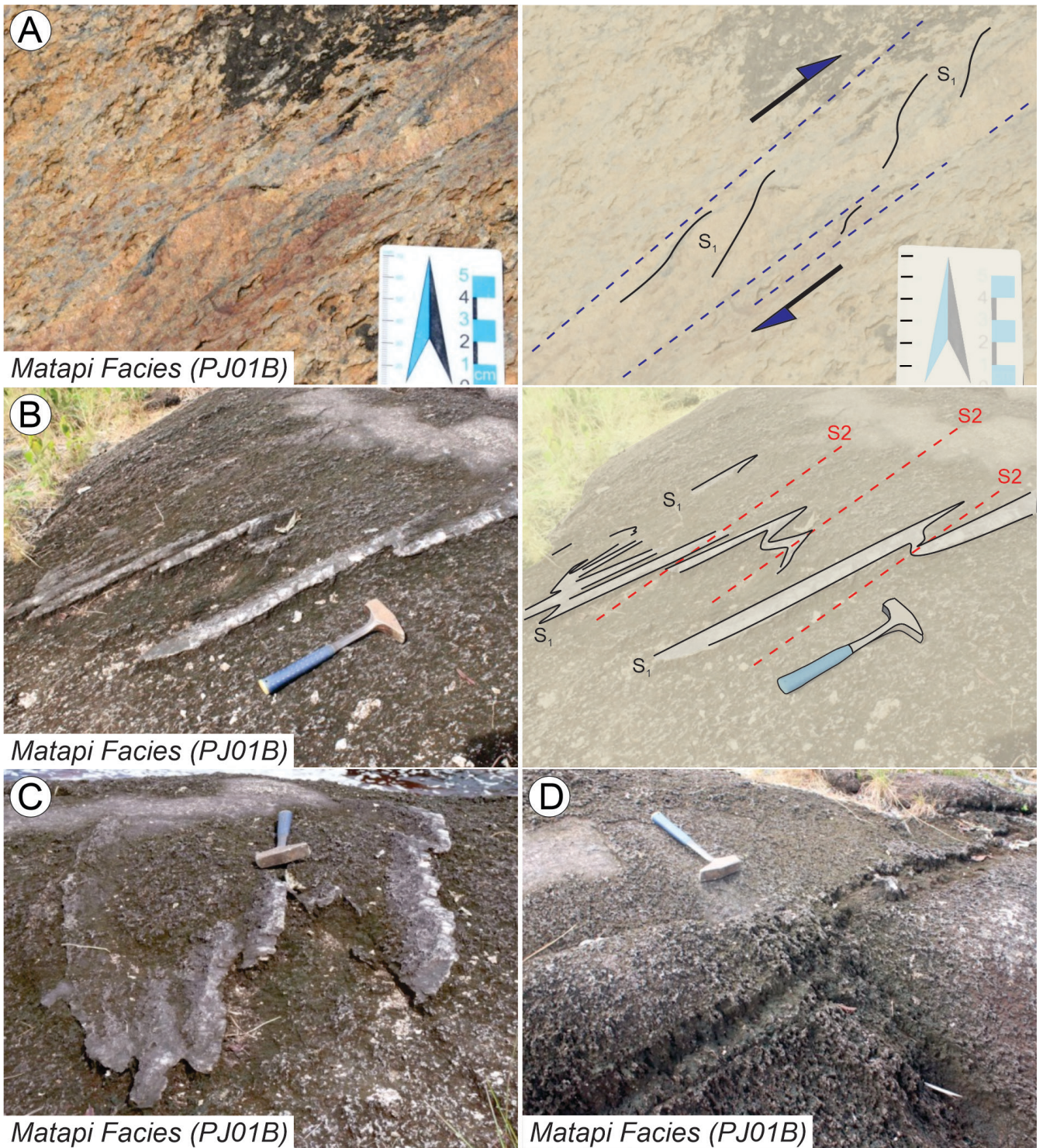
FIGURE 5. Mesoscopic aspects of deformed granites of the Querari Complex. (a) Ultramylonite bands with sinistral kinematic development of S1 foliation of the Matapi Facies; (b) Folded quartz veins parallel to the S_1 foliation showing the S_2 foliation as the axial plane of the folds (PJ01B); (c) Front view of quartz veins, parallel to the S_1 foliation, which were deformed to produce asymmetrical and tight folds with the S_2 foliation as the axial plane (PJ01B); (d) Folded pegmatite dike parallel to the S_1 foliation, showing internal S_2 foliation (PJ01B).
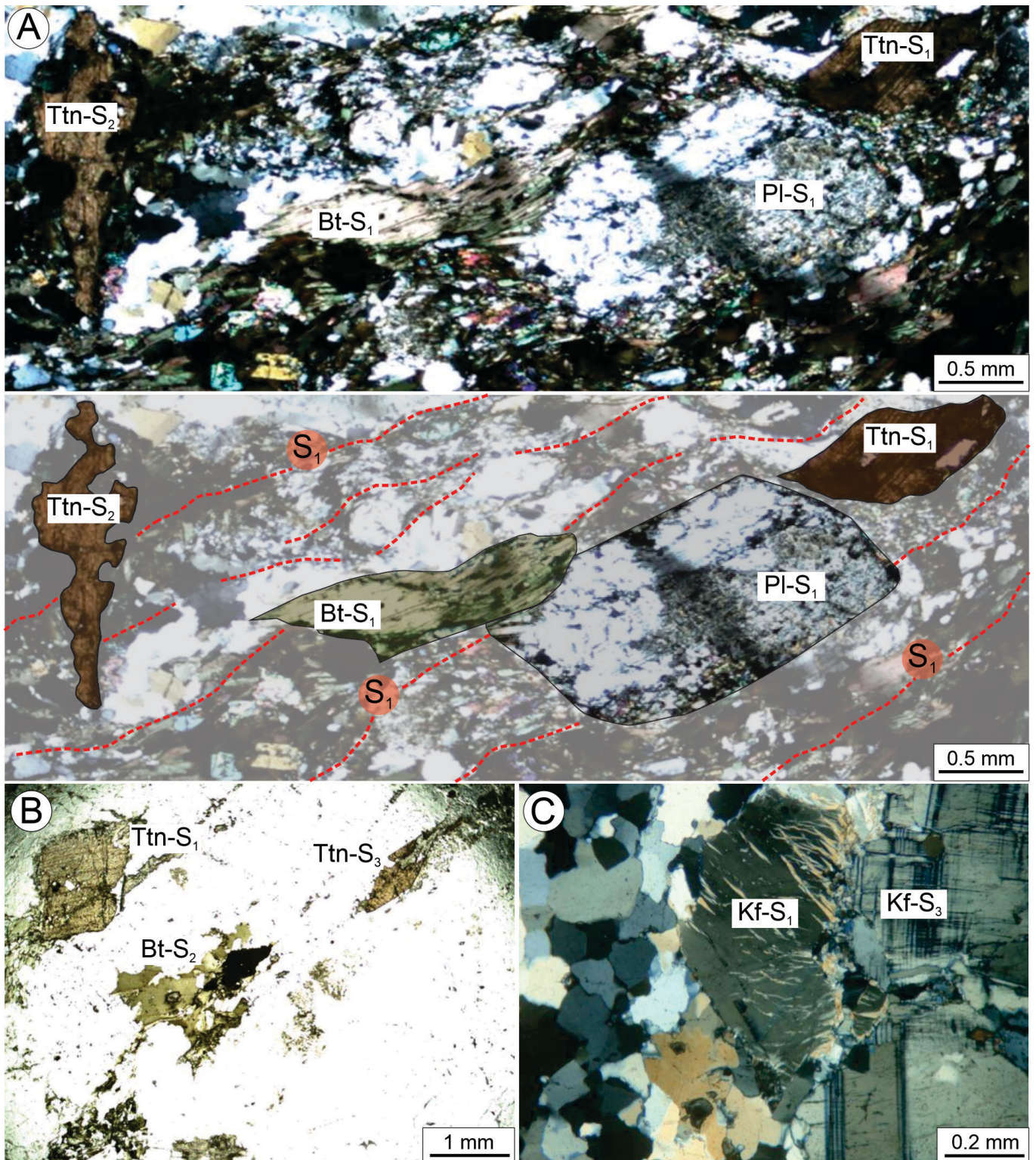
FIGURE 6. Microstructures of the deformed granites of the Panã-Panã Facies. (a) Smoothly crenulated S_1 foliation defined by plagioclase (Pl-S_1), biotite (Bt-S_1) and titanite (Ttn-S_1), and titanite porphyroblast (Ttn-S_2) axial plane to the S_1 crenulation (PJ03); (b) Deformed magmatic titanites (Ttn-S_1) parallel to euhedral titanite (Ttn-S_3), also, sigmoidal biotite according to S_2 foliation indicating parallelism between S_1 and S_3 foliations (PJ03); (c) Porphyroclast of K-feldspar (Kf-S_1) with dissolved edges and perthite in flame parallel to K-feldspar porphyroblast (Kf-S_3) showing the parallelism between S_1 and S_3 foliations (PJ03).
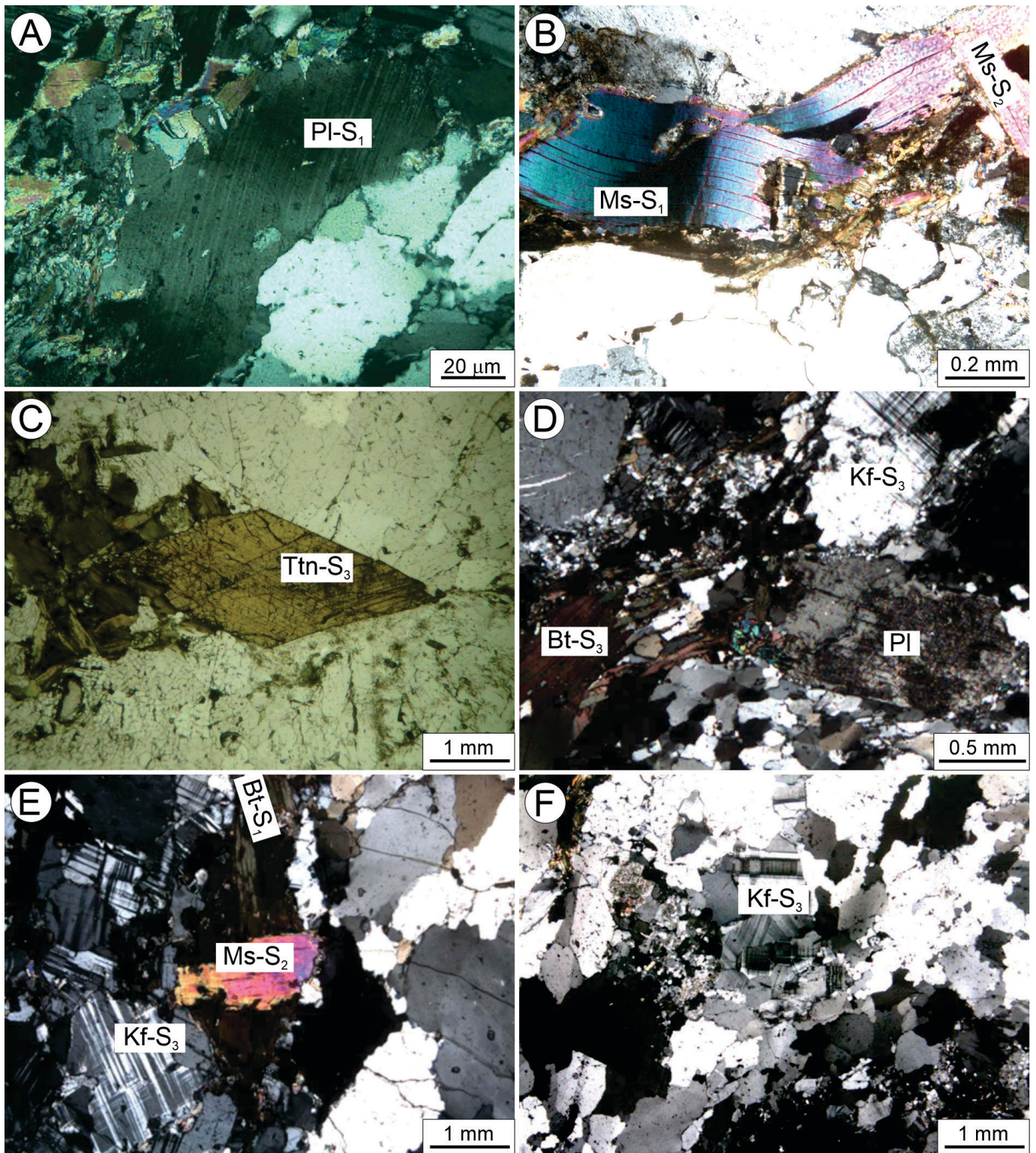
FIGURE 7. Microstructures characteristic of deformed granites of the Querari Complex. (a) Porphyroclast of plagioclase (Pl-S_1) with deformation twinning and interlobate boundaries with quartz of the Matapi Facies (PJ01B); (b) Matapi metagranite showing the S_1 foliation defined by kinked muscovite (Ms-S_1) and biotite. A muscovite (Ms-S_2) truncating S_1 foliation (PJ01B); (c) Porphyroblast of titanite (Ttn-S_3) in detail from the Panã-Panã Facies (PJ03B); (d) Porphyroblast of K-feldspar (Kf-S_3) according to S_3 foliation of the Panã-Panã Facies (PJ03B); (e) Muscovite (Ms-S_2) with corroded edges and porphyroblast of K-feldspar (Kf-S_3) without deformation of gneiss from the Matapi Facies (PJ01B); (f) A K-feldspar without deformation in the gneiss matrix from the Panã-Panã Facies (PJ03C).

lower SiO_2 contents (67.5 to 70.1 wt.% - 71.1 to 73 wt.%) and high contents of Al_2O_3 (13.55 to 16.85 wt.% - 14.5 to 15.15 wt.%), Fe_2O_3 (2.63 to 4.19 wt.% - 1.22 to 2.26 wt.%), MgO (0.34 to 1.17 wt.% - 0.08 to 0.55 wt.%), CaO (1.55 to 2.32 wt.% - 0.5 to 1.31 wt.%), Sr (137 to 205 ppm - 31.1 to 142 ppm), and Ba (492 to 1080 ppm - 51.6 to 438 ppm) (Table 1). These geochemical differences can be seen in the Harker variation diagrams (Fig. 8), and it can be implied that they reflect different source compositions or evolutionary processes for rocks the Panã-Panã and Matapi facies.

The deformed granites from Panã-Panã Facies are metaluminous with A/CNK values (molar Al_2O_3/CaO + Na_2O + K_2O) ranging between 0.91 and 0.99, except for three samples that plotted in the peraluminous field (PJ07, PJ10, and PJ11; Fig. 9a). The Matapi Facies contains muscovite as a primary mineral and show peraluminous character with A/CNK values ranging between 1.04 and 1.20 (Fig. 9a). The rocks of the Querari Complex are characterized by a high content of alkalis (Na_2O + K_2O) ranging between 7.76 to 9.11 wt.% in the Panã-Panã Facies and 8.14 to 9.53 wt.% in the

Table 1. Major and trace elements data of deformed granites of the Querari Complex.

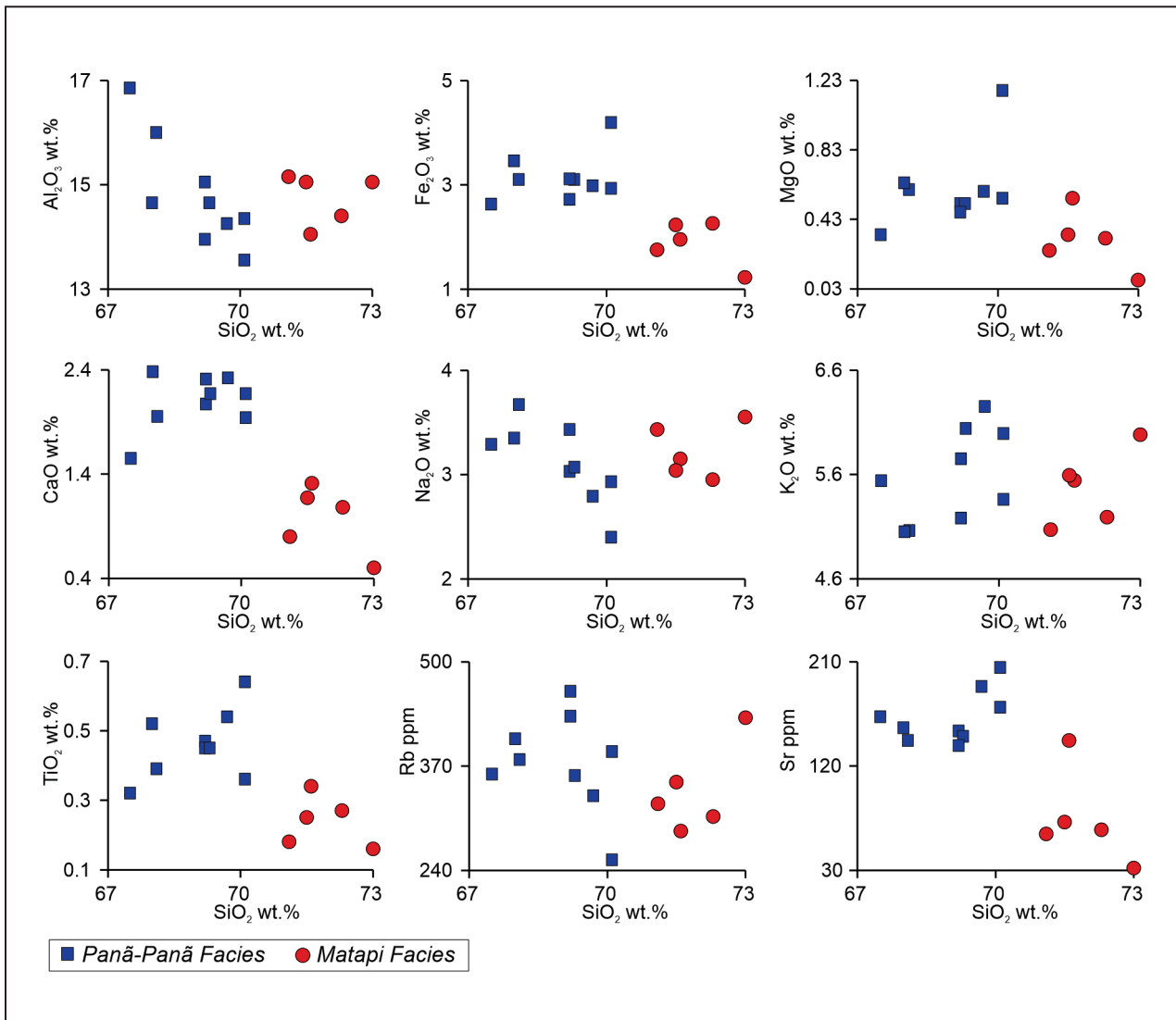| Sample PJ-	Panã-Panã Facies									Matapi Facies				
	10	13B	11	07	06A	12	14	03	06B	01B	01A	05	02	04
Major elements (wt.%)														
SiO_2	67.5	68.0	68.1	69.2	69.2	69.3	69.7	70.1	70.1	71.1	71.5	71.6	72.3	73
TiO_2	0.32	0.52	0.39	0.45	0.47	0.45	0.54	0.36	0.64	0.18	0.25	0.34	0.27	0.16
$Al2O_3$	16.85	14.65	16	15.05	13.95	14.65	14.25	13.55	14.35	15.15	15.05	14.05	14.4	15.05
Fe_2O_3	2.63	3.46	3.1	2.72	3.11	3.1	2.98	2.93	4.19	1.75	2.23	1.95	2.26	1.22
MnO	0.05	0.1	0.08	0.08	0.1	0.09	0.07	0.07	0.1	0.06	0.08	0.04	0.06	0.03
MgO	0.34	0.64	0.6	0.52	0.47	0.52	0.59	1.17	0.55	0.25	0.34	0.55	0.32	0.08
CaO	1.55	2.38	1.95	2.07	2.31	2.17	2.32	2.17	1.94	0.8	1.17	1.31	1.08	0.5
Na_2O	3.29	3.35	3.67	3.43	3.03	3.07	2.79	2.4	2.93	3.43	3.04	3.15	2.95	3.55
K_2O	5.54	5.05	5.06	5.18	5.75	6.04	6.25	5.36	5.99	5.07	5.59	5.54	5.19	5.98
P_2O_5	0.05	0.25	0.18	0.28	0.25	0.2	0.2	0.12	0.24	0.08	0.08	0.07	0.09	0.01
P.F	1.84	1.36	1.21	1.34	1.21	1.03	0.92	1.09	0.92	1.2	0.98	1.11	1.14	1.31
Total	100.05	99.84	100.41	100.4	99.95	100.72	100.75	99.41	101.95	99.12	100.37	99.78	100.12	100.92
Trace elements (ppm)														
Ba	650	547	492	556	703	728	960	560	1080	247	377	438	356	51.6
Rb	360	404	378	432	463	358	333	253	388	323	350	289	307	430
Sr	162.5	153	142	150	137.5	145.5	188.5	205	170.5	61.3	71.5	142	64.8	31.7
Hf	15.4	18.6	18.6	16.7	19.3	13.1	22.6	9.3	12.9	4.5	7.3	6.7	7.5	2.7
Nb	35.3	53.8	47.9	56	63.2	35.3	36.5	14	54.3	26.9	20.4	23.2	22.9	44.4
Ta	2.6	5	4	5	5.1	2.3	2.3	1.3	4.7	4.6	2.1	1.9	2.6	5.8
Th	123.5	125	127	131.5	90.6	81.4	25.4	63.7	39.7	16.45	24.9	47.7	28.5	61.8
U	15.8	21.1	29	21.6	29.4	11.9	3.27	14.95	10.85	2.93	8.5	18.6	11.45	26.7
V	27	35	34	30	31	25	36	50	40	12	18	24	19	9
Ga	27.2	25.9	27.8	26	24	24.1	23.1	18.3	25.1	20.1	21.6	20.4	21.9	20.4
Zr	500	611	573	508	616	435	806	279	448	124	215	192	200	51
Y	74	156	137.5	137	133	115	97	61.8	137	45	135.5	217	283	49.8
Cr	130	140	130	100	140	120	110	120	260	160	130	130	140	100
Sn	4	11	6	10	10	4	5	2	7	3	6	5	6	4
Cs	4.69	6.37	6.8	7.33	13.9	6.63	3.23	9.07	4.61	19.35	31	11.1	29.5	15.95
La	253	290	285	179	165.5	206	128.5	80.5	123.5	22.5	66.2	359	286	16.8
Ce	701	559	514	292	339	377	276	146.5	248	47	131	644	419	38.3
Pr	57.9	66.2	61.6	41	37.4	44.7	32.7	16.25	31.7	5.62	16.85	74.1	48.1	4.46
Nd	185.5	229	209	140.5	133.5	149	125.5	56.6	118	20.5	61.7	255	175.5	15.6
Sm	25.1	34.8	32.2	23.9	24	24.6	22.5	9.21	22.3	4.28	14.1	40.8	34.4	3.28
Eu	2.25	3.15	2.56	2.44	2.25	2.32	2.88	1.36	2.46	0.46	1.71	4.58	4.44	0.18
Gd	15.45	28.1	27.3	21	22.6	21.4	19.55	9.21	22	5.08	18.55	36.2	40.2	3.94
Tb	2.23	4.04	3.88	3.2	3.47	2.96	2.82	1.3	3.3	0.92	3.2	5.48	5.93	0.76
Dy	11.9	23.4	21.9	19.55	20.8	17.6	15.8	8.08	19.65	6.54	20.6	31.4	34.6	5.88
Ho	2.41	4.91	4.47	4.31	4.69	3.8	3.31	1.92	4.41	1.55	4.62	6.64	6.97	1.55
Er	7.26	15.25	13.15	13.65	14.1	10.9	9.71	5.68	13.75	4.88	13.75	19.9	19.2	5.73
Tm	1.09	2.39	1.98	2.07	2.1	1.55	1.42	0.82	2.07	0.74	1.99	2.8	2.62	0.97
Yb	7.94	18.9	14.65	15.95	15.7	10.6	10.05	6.09	15.35	5.48	13.75	19.8	17.65	7.27
Lu	1.08	2.7	2.06	2.14	2.3	1.55	1.38	0.89	2.11	0.73	1.88	2.63	2.32	1.06
SREE	1274.1	1281.8	1193.7	760.7	787.4	873.9	652.1	344.4	628.6	126.2	369.9	1502.3	1096.9	105.7
(La/Yb)n	21.48	10.34	13.12	7.57	7.11	13.10	8.62	8.81	5.42	2.77	3.25	12.22	10.92	1.56
(Ce/Yb)n	22.84	7.65	9.08	4.74	5.59	9.20	7.10	6.22	4.18	2.22	2.46	8.41	6.14	1.36
(Gd/Yb)n	1.57	1.20	1.50	1.06	1.16	1.63	1.57	1.22	1.16	0.75	1.09	1.48	1.84	0.44
Eu/Eu*	0.33	0.30	0.26	0.33	0.29	0.30	0.41	0.45	0.34	0.30	0.32	0.36	0.36	0.15

FIGURE 8. Harker diagrams using SiO_2 as the difference index, showing geochemical behavior in terms of major and trace elements for deformed granites of Matapi and Panã-Panã facies.

Matapi Facies. Both facies have calc-alkaline rock signature (Fig. 9b, 9c, 9d).

On the Chondrite REE diagram (Fig. 10a), the Panã-Panã Facies exhibit enrichment of the LREE in comparison to HREE $((La/Yb)_N = 5.42–21.48)$. There is a high degree of LREE fractioning in the Panã-Panã Facies rocks $((La/Sm)_N = 3.48–6.34)$. On the contrary, the HREE in these rocks is weakly fractionated $((Gd/Yb)_N = 1.06–1.63)$. Eu anomaly is deeper negative $(Eu_{(N)}/Eu^* = 0.21-0.45)$. The metagranites of the Matapi Facies show major heterogeneity on the REE distribution pattern (Fig. 10b). REE-rich samples (PJ02 and PJ05) show a more fractionated pattern $((La/Yb)_N = 10.92$ and 12.22, respectively), compared to the rest of the samples, which display a more horizontal pattern $((La/Yb_N = 1.56–3.25)$. However, there was no significant variation in the negative Eu anomaly $((Eu_{(N)}/Eu^*) = 0.15–0.36)$. On the Chondrite-normalized multi-elementary diagram, the samples of the Panã-Panã Facies exhibit negative anomalies for Nb, Sr, P, and Ti, and positive anomalies for Th, La, Ce, and Nd (Fig. 11a). The Matapi Facies is characterized by negative anomalies for Nb, Sr, P, and Ti and positive anomalies for Nd and variable anomalies for La, Ce, and Sm (Fig. 11b).

5. Discussions

5.1. Petrogenesis of the Panã-Panã and Matapi facies

The rocks of the Querari Complex are generally enriched in silica, and have a small spectrum of variation (Table 1, Fig. 8). The Panã-Panã deformed granites are metaluminous rocks with ASI <1.1 (Fig. 9a), have a high content of Na_2O, CaO, Fe_2O_3, Ba and Sr (Table 1), have biotite and titanite as the main mafic minerals and, therefore, are more similar to I-type granites (Chappell and White 1974, 2001). On the other hand, the rocks of the Matapi Facies have biotite and muscovite as igneous minerals (two-mica granites), ASI >1.1 (Fig. 9a), high K_2O and Al_2O_3 and low CaO and Fe_2O_3 (Table 1). These characteristics are more compatible with S-type granites.

I-type granites can result from the partial melting of crustal rocks, of basic to intermediate composition, or also by mantle sources (Kemp et al. 2007); on the other hand, S-type granites are commonly interpreted to be derived from upper-crustal metasedimentary sources (Chappell and White 1974). Taking into account the regional context and the geochemical characteristics of the rocks from the Panã-Panã and Matapi
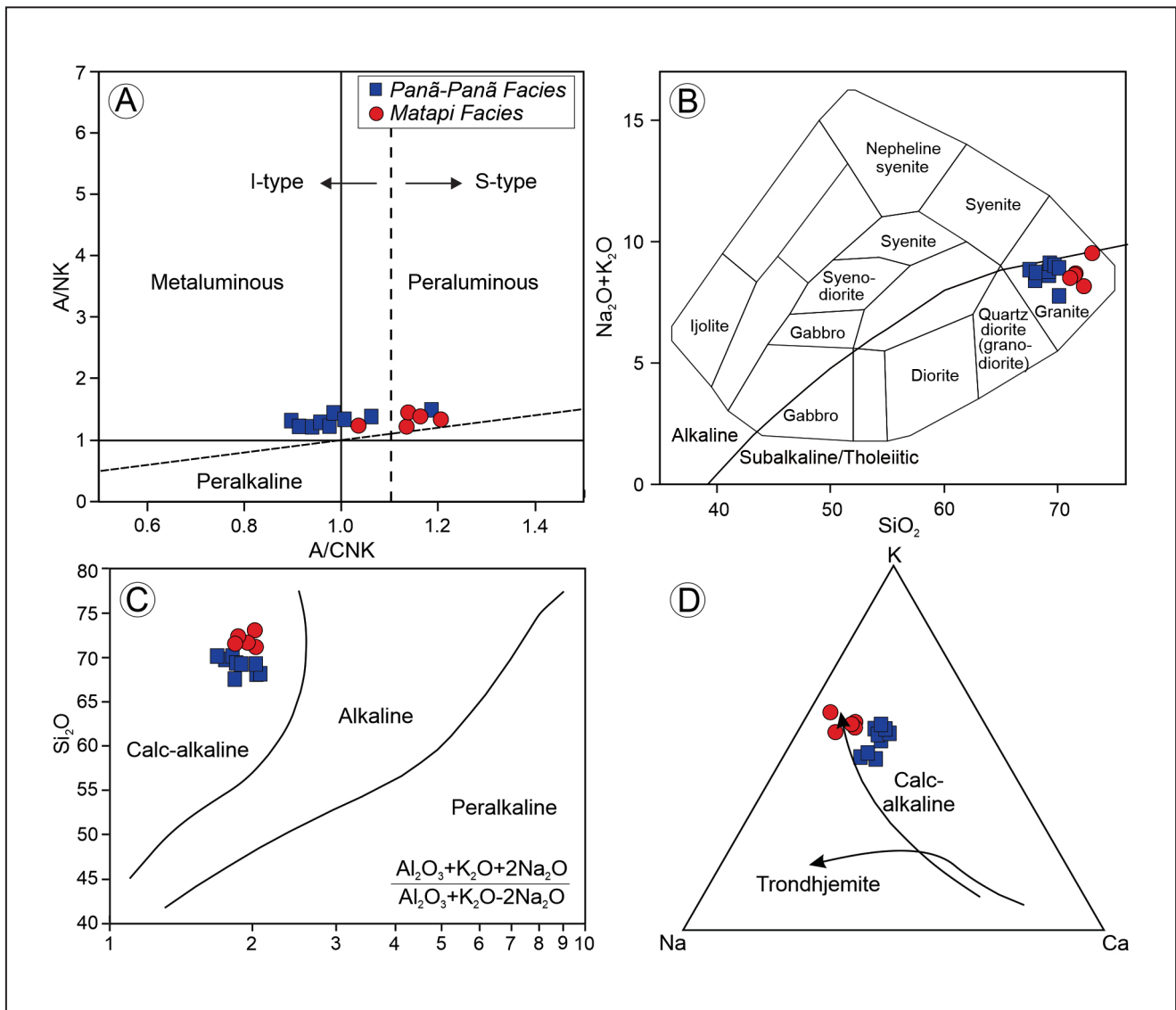
FIGURE 9. Major element geochemistry for the rocks of the Panã-Panã and Matapi facies. (a) Aluminum saturation index (Shand 1927) A/CNK (molar $Al_2O_3/CaO + Na_2O + K_2O$) versus A/NK (molar $Al_2O_3/Na_2O + K_2O$). Discrimination fields for different types (e.g., I-type and S-type) of granitoid rocks (Maniar and Piccoli 1989); (b) Nomenclature of plutonic rocks using the TAS (total alkali-silica) diagram (according to Cox et al. 1979). The dividing line between alkaline and subalkaline/tholeiitic magma series is from Miyashiro (1978); (c) Alkalinity diagram versus SiO_2 (Wright 1969); (d) Na–K–Ca diagram confirming calc-alkaline affinity of the Panã-Panã and Matapi facies. The trondhjemite and calc-alkaline trends were defined by Barker and Arth (1976).

facies, we suggest a crustal source for the origin of these rocks. However, two distinct crustal sources may be the case here.

Comparing the study rocks with those of the experimental fields defined by Patiño Douce (1999) and Laurent et al. (2014) for sources of granitic rocks, the rocks of Matapi Facies would be derived from partial melting of metasedimentary rocks (metagraywacke and/or metapelitic; Fig 12, 13). The field information corroborates this hypothesis (metasedimentary source), since in the Matapi Facies, a quartzite xenolith was identified in the outcrop. Also, the presence of magmatic muscovite and biotite, normative corundum higher than 1% (1.85-2.06), and the high peraluminous character of the Matapi Facies strongly suggest a metasedimentary source for these rocks.

On the Patiño Douce (1999) diagram, the rocks of Panã-Panã Facies plot in the field of amphibolite melts (Fig. 12), while on the ternary diagram from Laurent et al. (2014), these

rocks plot in the field of metasedimentary source (Fig. 13) together with the Matapi Facies. Importantly, the rocks of the Panã-Panã Facies are granites (*stricto sensu*), feldspar-rich but poor in ferromagnesian minerals; consequently, they have small amounts of ferromagnesian oxides ($FeO_t + MgO + MnO + TiO_2 = 3.08 - 5.06$ wt.%) and CaO (1.55 – 2.38 wt.%) and high alkalis ($Na_2O + K_2O = 7.76 - 9.11$ wt.%) and Al_2O_3 (13.55 – 16.85 wt.%). Due to these geochemical characteristics, especially the low CaO and high alkalis, the Panã-Panã Facies plots in the field of metasedimentary sources (Fig 13). However, there is a tendency towards the field of high-K mafic rocks. The mineralogy and chemical signature of these rocks are not consistent with the hypothesis of metasedimentary sources. Many high-K calc-alkaline granites (monzogranite/syenogranite) are interpreted as the melting product of low-pressure (plagioclase stable) (± garnet) crustal source of intermediate composition, such as a composition of tonalitic
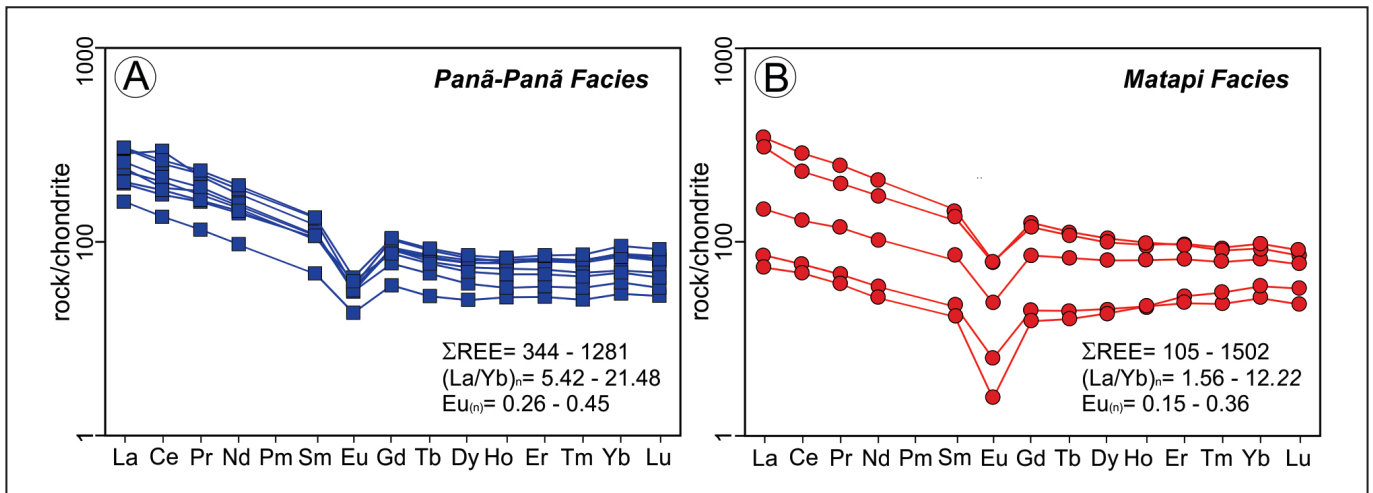
FIGURE 10. Chondrite-normalized REE patterns for the samples of the Querari Complex. Normalized values are given by Boynton (1984): (a) Panã-Panã Facies; (b) Matapi Facies.
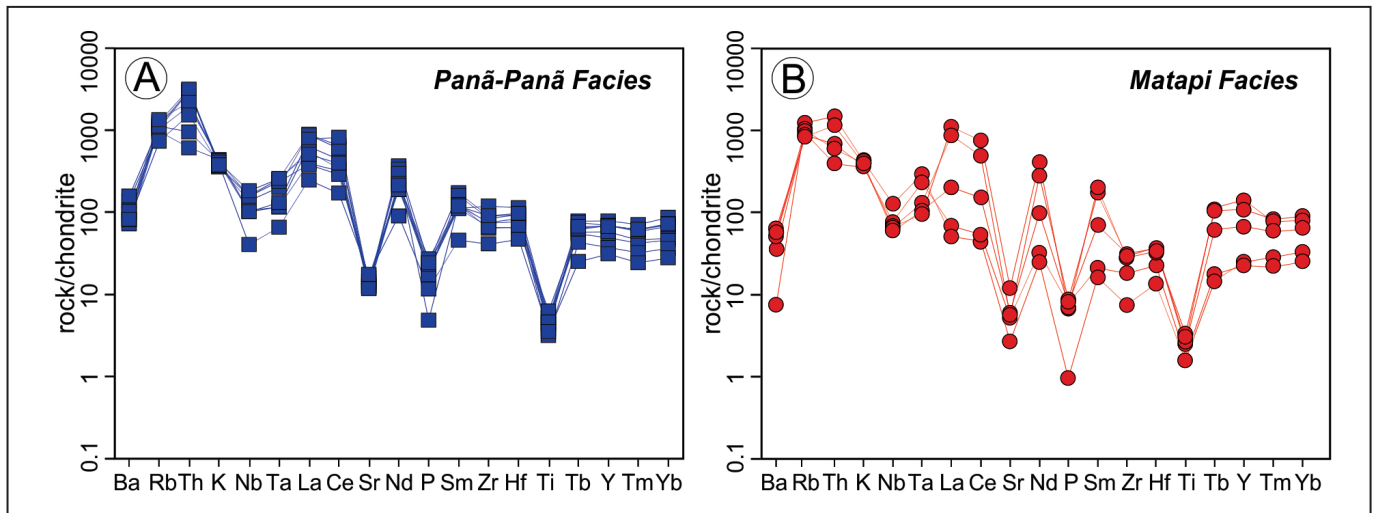

FIGURE 11. Chondrite-normalized multi-element spider diagrams for the samples of the Querari Complex. Normalized values are given by Thompson (1982): (a) Panã-Panã Facies; (b) Matapi Facies.

gneisses (e.g., Liégeois et al. 1998, Jayananda et al. 2006, Shang et al. 2010, Laurent et al. 2014, Manya and Moboko 2016, Tulibonywa et al. 2017, Li et al. 2019). Therefore, we suggest that the Panã-Panã Facies derived from partial melting of meta-ignea source of intermediate composition, such as composition tonalitic gneisses.

Regarding the processes involved in the genesis of protoliths these rocks, we infer for the Panã-Panã Facies that fractional crystallization processes could probably have played a role on its evolution. In the Harker variation diagrams, despite the small SiO_2 variation interval, some slight evolutionary trends can be seen for the Panã-Panã Facies (Fig. 8). Also, the Eu anomaly suggests the fractionation of plagioclase (Fig. 10a), and diagrams correlating incompatible elements (Fig. 14) point to fractional crystallization as the main process involved in the genesis of these rocks. For the rocks of the Matapi Facies, the involvement of fractional crystallization processes is inconclusive, which may be attributed to the small number of samples and the restricted range of SiO_2 (1.9 wt.%). However, rocks of the Matapi Facies also have the pronounced negative Eu anomaly (Fig. 10b), which may be

related to fractional crystallization of plagioclase and/or the presence of plagioclase as stable restite in the source of melt.

5.2. Regional correlation and tectonic interpretation

The geochemical differences among the study rocks have brought up the need for a distinction of the Querari Complex into two facies. The Panã-Panã Facies comprises deformed granites, with syeno to monzogranitic composition, metaluminous character, and calc-alkaline affinity, correlated with the Querari Lithofacies (Almeida 2006) or the Querari Complex (Almeida et al. 2013). However, the Matapi Facies comprises two-mica deformed granites with calc-alkaline and peraluminous affinities, which has no equivalent in previous literature. In the study area (Fig. 1c), A-type granites of Tiquié Intrusive Suite (Almeida 1997) have been mapped by Almeida (2006), and they were further defined as indiscriminate granitic intrusions (Almeida et al. 2013). Nevertheless, neither the petrographic nor the geochemical characteristics of these rocks seem to represent the Matapi Facies. Contrasting with Matapi Facies, the Tiquié granites show: (i) mineralogy
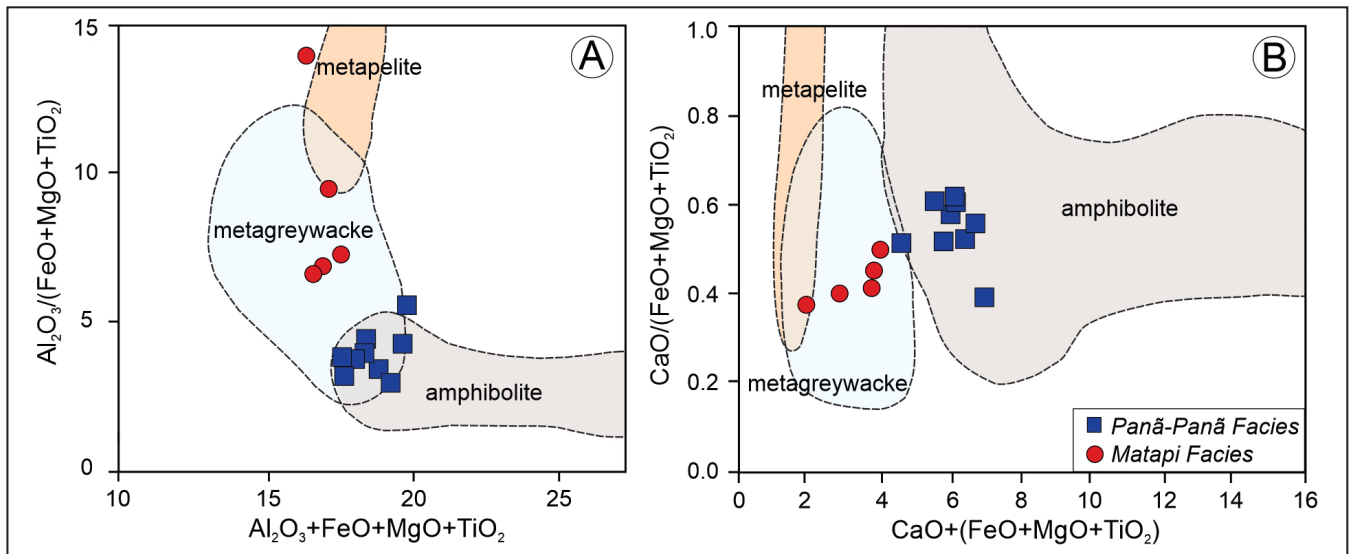
FIGURE 12. Comparison of the Querari Complex rocks with the melt compositions produced by experimental melting by dehydration of amphibolite, metagreywacke, and metapelite according to Patiño Douce (1999).
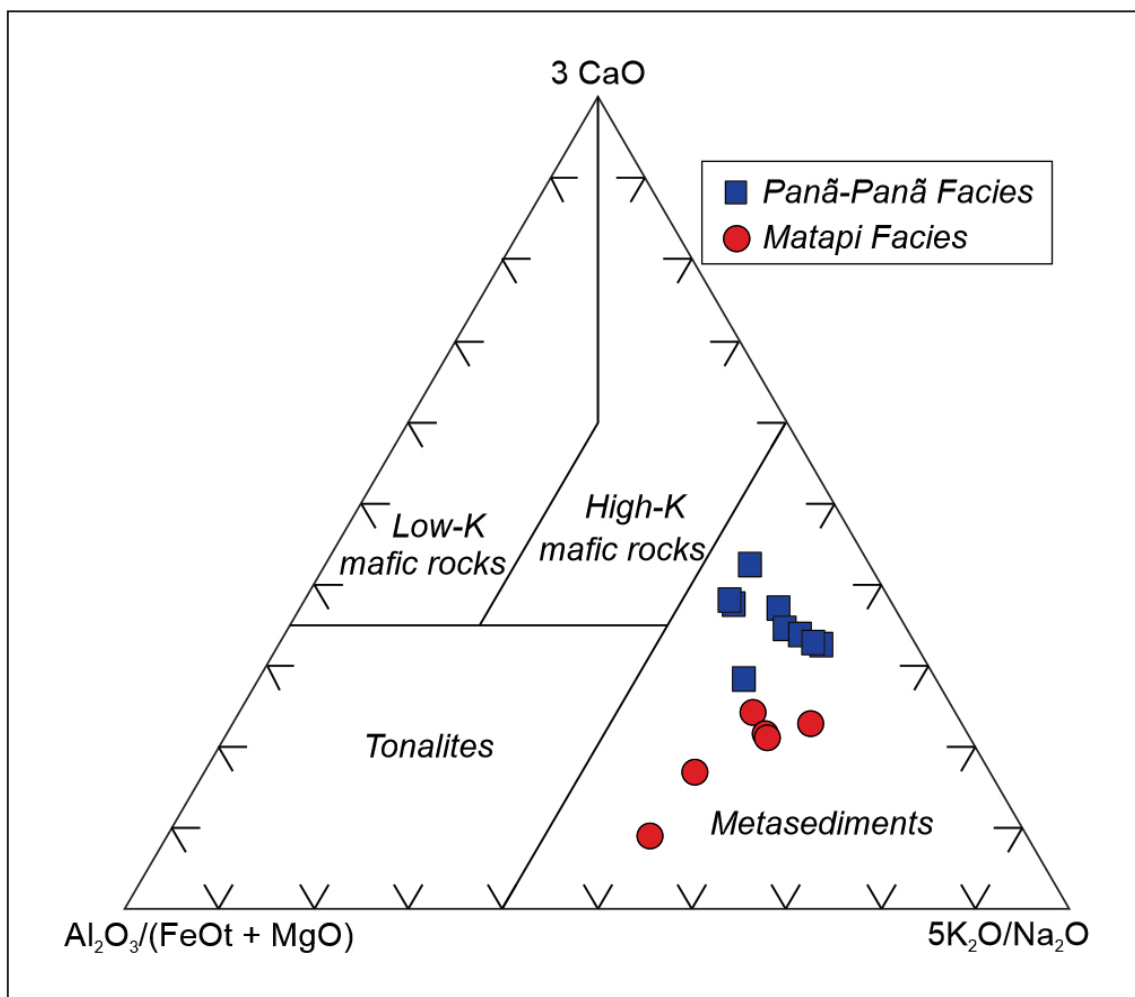

FIGURE 13. Magmatic facies of the Querari Complex plotted in the $Al_2O_3/(FeO_t + MgO)$; $3CaO$; $5(K_2O/Na_2O)$ diagram (Laurent et al. 2014). The fields represent the composition of melts derived from tonalites, metasediments, low- and high-k mafic protoliths.
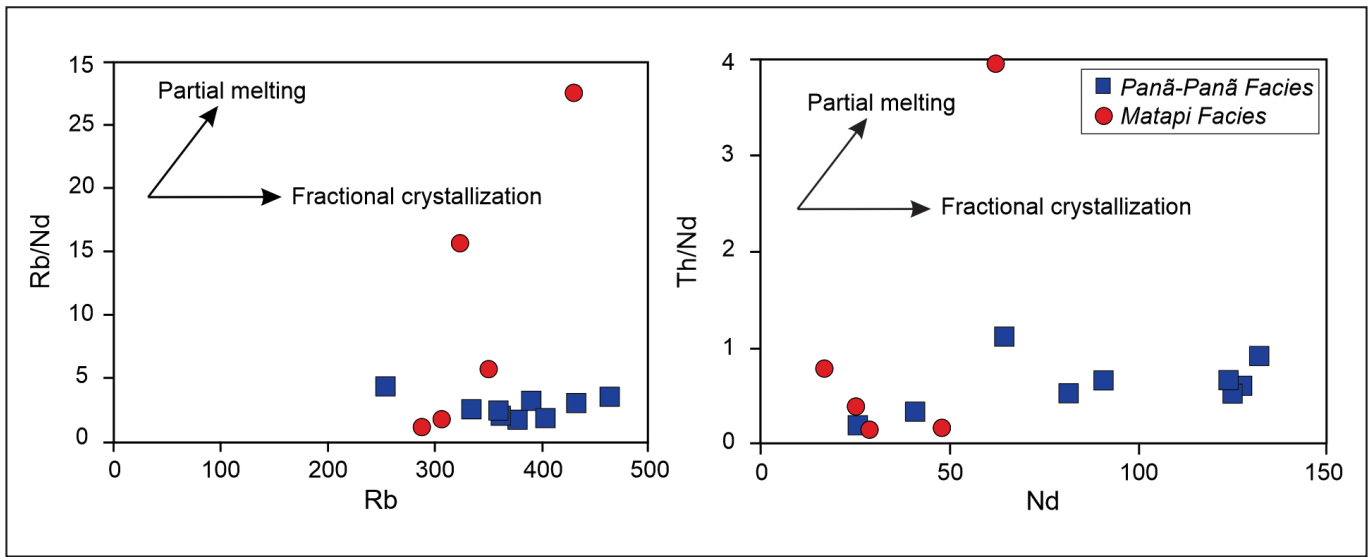
FIGURE 14. Schematic diagram of (a) Rb/Nd versus Rb and (b) Th/Nd versus Nd of the Querari Complex according to Schiano et al. (2010).

represented by titanite, hornblende, allanite, and fluorite; (ii) muscovite absence; (iii) high SiO_2 content (70 to 76 wt.%); and (iv) metaluminous character. These aspects are more compatible with deformed granites of the Panã-Panã Facies that outcrop at Caranguejo Mountain (Fig. 1c).

A possible unit related to the Matapi Facies was described by Mendes et al. (2020) in the east part of the study area, which they named as Igarapé Tocandira Granite. This unit intrudes rocks of the Taiuaçu-Cauera Complex. The results presented here are based on two samples studied by Mendes et al. (2020). These are inequigranular meta-syenogranites and may present phenocrysts of K-feldspar, biotite and muscovite as the main igneous minerals. The rocks have relatively high contents of SiO_2 (69.1 and 71.8 wt.%) and K_2O (5.63 and 4.73 wt.%), low contents of Na_2O (2.42 and 2.97 wt.%) and CaO (1.39 and 2.16 wt.%) and moderately low contents of Al_2O_3 (14.10 and 14.80 wt.%). Geochronological data presented by Mendes et al. (2020), reveled U-Pb in zircon (SHRIMP) of 1816 Ma, 1810 Ma, 1790 Ma, and 1771 Ma. These authors interpret the age of 1790 Ma as the age of crystallization and 1771 Ma as the age of metamorphism. The oldest zircons are interpreted as xenocrysts derived from the Taiuaçu-Cauera Complex. The geochemistry of the Igarapé Tocandira Granite presented by Mendes et al. (2020) is similar to that the Panã-Panã Facies and age consistent with those that were obtained for the basement rocks. However, in this work, we suppose that the age of 1771 Ma would represent the age of crystallization, and do not represent metamorphic age as presented by Mendes et al. (2020). The 1771 Ma age as a magmatic event would be more coherent with the field and micro-textural data obtained in this work and by Veras et al. (2018) in the Taiuaçu-Cauera rocks.

According to the ages obtained for the extreme north-western region of Amazonian Craton (Brazil, Colombia, and Venezuela area), which have been summarized by Cordani et al. (2016), it can be inferred that the igneous protoliths of the Querari Complex have been generated between 1780 and 1740 Ma from slightly juvenile sources with εNd(t) between -0.51 and 0.45, and model ages between 2.0 and 2.2 Ga. The Sm-Nd isotopic data demonstrated by Cordani et al. (2016) may be related to Panã-Panã granites, despite the brief description of the study rocks.

Cordani et al. (2016) have inferred that basement rocks were generated between 1800 and 1740 Ma (Atapabo Belt) in a long-lived magmatic arc environment with the subduction of an oceanic plate under the cratonic area created by the Venturari-Tapajós continent. Almeida et al. (2013) attributed the ages of 1740 and 1703 Ma to the igneous protoliths of the Querari Complex, which were formed in an island arc environment (Querari Orogeny).

The rocks of the Querari Complex studied in this work plot in the collision-related peraluminous field of the Zr versus $(Nb/Zr)_N$ diagram of Thiéblemont and Tegyey (1994; Fig 15a). In the Rb-Hf-Ta triangular (Harris et al. 1986), the samples from the Panã-Panã Facies lie in the volcanic arc field (Fig. 15b). The deformed granites from the Matapi Facies plot in the late to post-collisional field from the same diagram (Fig. 15b).

The structural data indicate that the Matapi and Panã-Panã magmas are syn-tectonic (D_1), emplaced during the development of the S1 foliation, with NE-SE direction, parallel to the magmatic S_0 foliation. After the generation and emplacement of the igneous protoliths, a secondary tectonic event (D_2) has been registered. This D_2 event was responsible for the folding of the S_1 foliation and the development of the S_2 axial planar foliation, with E-W approximate direction. Deformation textures and mineral paragenesis point to an upper amphibolite metamorphic event, around 700°C.

The D_2 event may be related to the Parguazan event (Priem et al. 1982), registered in Brazil, Colombia and Venezuela as a high-grade metamorphic event with associated plutonism, which occurred between 1560 and 1450 Ma. In the Brazil territory, this event is called Içana Orogeny (Almeida et al. 2013), interpreted as a collisional orogen (arc-collision) responsible for the generation of I- and S-type granites between 1540 and 1480 Ma in the Rio Negro Province. Cordani et al. (2016) have also recognized an orogenic event (continental magmatic arc) between 1580 and 1520 Ma that has been responsible for the formation of the Vaupés Belt.

Mineral paragenesis and textures associated with the S_3 foliation also fit in a high-grade metamorphic event with temperature up to 700°C, reaching the anatexis isograde. Ar-Ar isotopic data, mainly on micas, indicated regional heating up to 400°C between 1400 and 1100 Ma (Cordani et al. 2016),
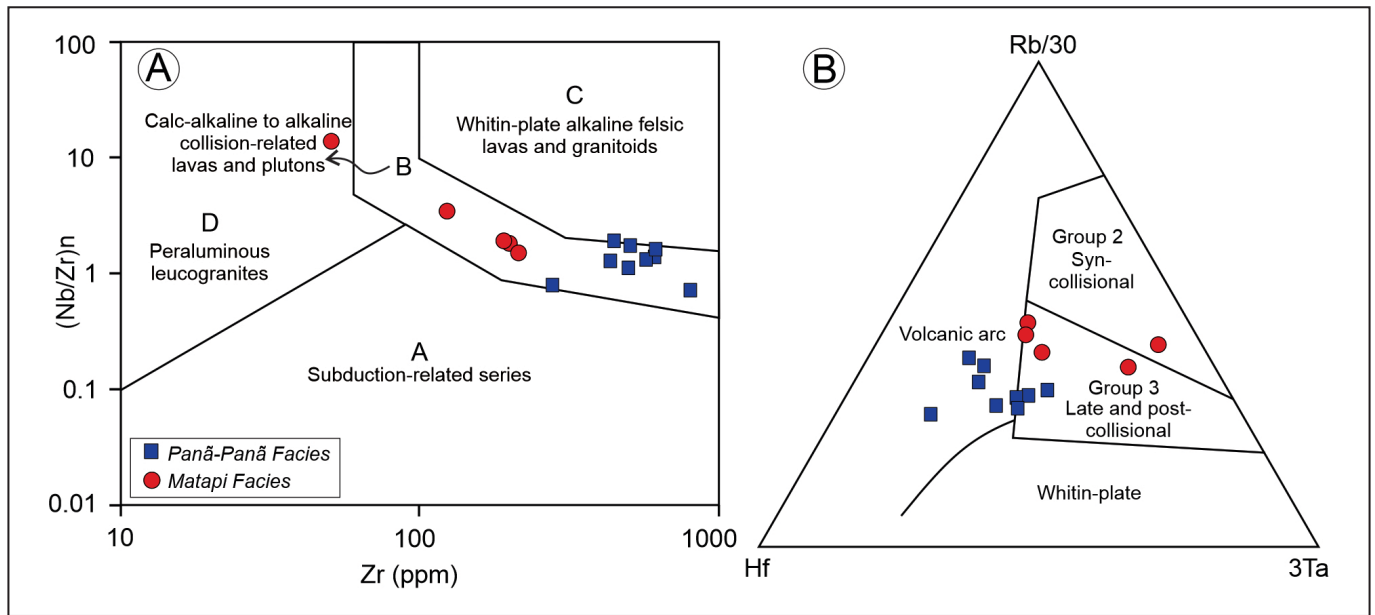
FIGURE 15. Discriminating diagrams of tectonic environments for the rocks of the Querari Complex. (a) Zr versus $(Nb/Zr)_N$, diagram for the geotectonic discrimination of the differentiated magmatic rocks (Thiéblemont and Tégyey 1994). Normalization to the Primordial Mantle, mean values of Hofmann (1988): Zr = 9.714 ppm and Nb = 0.6175; (b) The Hf-Rb-Ta discrimination diagram by Harris et al. (1986).

with a higher frequency between 1350 and 1250 Ma (Priem et al. 1982). This younger heating process has been related to a low-temperature metamorphic event (Nikerie Event; Priem et al. 1971 or K´Mudku; Gibbs and Barron 1993). However, Santos et al. (2006) argued that K´Mudku corresponds to a high grade metamorphic event (amphibolite facies and locally granulite), based on U-Pb ages obtained through the Rio Negro Province (Imeri Domain), with zircon and titanite ages of the Tapajós-Parima between 1.49 and 1.15 Ga. According to Santos et al. (2008), the Sunsás orogeny would be fragmented into four pulses: Santa Helena between 1.47 and 1.43 Ga; Candeias between 1.37 and 1.32 Ga; Santo André around 1.27 Ga and Nova Brasilândia between 1.19 and 1.11 Ga.

In Colombia, the high-grade basement rocks exposed in the northern Andes, and the buried basement of the adjacent Putumayo foreland basin, were strongly deformed during at least one metamorphic episode dated at 0.99 Ga (Ibanez-Mejia et al. 2015). Zircon U-Pb (inherited) and Hf-O isotopic studies, suggest an orogen (Putumayo) with an evolution based on an arc system in the early times (1470 Ma) and a shift in orogenic deformation style starting at ~1150–1100 Ma (Ibanez-Mejia et al. 2015).

The S_3 foliation presents a NE-SW parallel to S_1, which may be a consequence of the reactivation of older structures, as an effect of Sunsás (or Putumayo) Orogeny intracontinental reworking (Santa Helena pulse?). To clarify this question, isotopic studies need to be conducted on S_3 titanite. Finally, low-temperature textures indicate a tectonic-metamorphic event (M_4) on greenschist facies which are superimposed to the high-temperature textures. This M_4 event might be linked to the last stages of the K´Mudku event.

The subdivision of Rio Negro Province into distinct domains has been proposed by Almeida et al. (2013); each domain may represent distinct orogens with distinct evolutionary geodynamics. Geochemical and isotopic data from Almeida et al. (2013) and Carneiro et al. (2017) demonstrate different features for basement metagranitoids of the Rio Negro Province,

which could explain the subdivision into distinct domains. Nonetheless, the tectonic-metamorphic evolutionary pattern for Cauaburi Complex proposed by Carneiro et al. (2017) is similar to the one observed in the rocks of the Querari Complex. On the rocks of the Cauaburi Complex, three registered tectonic-metamorphic events have been recognized by Carneiro et al. (2017): D_1 event, responsible for S_1 foliation, which is linked to the 1.86 - 1.78 Ga syn-tectonic igneous protoliths with NE-SW trending foliations with sub-horizontal dips to SE. However, the $S_0//S_1$ foliation observed in syn-cinematic granites of the Querari Complex (1.75 - 1.72 Ga), are probably younger than the D_1 event described in the Imeri Domain (Cauaburi Complex 1.82 - 1.78 Ga). The D_2 event is responsible for the S_2 foliation developed under upper amphibolite facies oriented to NW-SW, simultaneously to Calymmian (1.52 - 1.48 Ga) I- and S-type granite emplacement. Finally, the D_3 event, which is responsible for NE-SW-trending mylonitic foliation, is associated with the development of transcurrent shear zones under greenschist conditions. These deformational-metamorphic effects are a consequence of the 1.26 - 1.14 Ga K´Mudku event and related to the last stages of the Putumayo Orogeny.

In this work, we suggest that, in the Querari Complex, three events have been recognized, and they must go through the following considerations: (i) the S_0 (magmatic) foliation parallel to the S_1 foliation with NE-SW direction; (ii): the S_2 foliation is oriented to ENW-WSW with a similar dip to the S_2 foliation of the Cauaburi Complex, and both of them have been created on upper amphibolite facies and; (iii) the last event reworks the older NE-SW structures, similarly to what happens at the Cauaburi Complex, but under high-temperature conditions.

A comparison between the rocks of Cauaburi and Querari complexes indicates that there are different sources and/ or evolutionary processes. The Cauaburi basement is older than the Querari Complex and shows gneisses and metagranitoids varying from banded to ovoid types. Their protolithic compositions are predominantly monzogranitic to granodioritic, locally tonalitic, and rarely dioritic. Anatexis

processes are also common in the Cauaburi domain, generating migmatites at different events. In the study area, the Querari Complex shows metagranitoids foliated to locally banded gneiss. Migmatites have not been found. However, structural and metamorphic data suggest a similar evolution for both complexes.

All data in this study suggest at least two hypotheses for a magmatic, structural and metamorphic evolution for this area of the Rio Negro Province: a) long-lived continental magmatic arc (Cordani et al. 2016), with the evolution from 1.80 Ga to 1.74 Ga, represented by I-type (and minor A-type) magmatic series (Cauaburi and Querari Complex; Almeida et al. 2013); b) Two different arc magmatic systems, represented by an older continental magmatic arc (1.83-1.76 Ga), and A-type post-orogenic granitoids (1.75 Ga), with strong crustal reworking (Tapajós-Parima Crust), and younger continental magmatic arc (1.75-1.70 Ga), with the generation of derived-mantle magmas and subordinate crustal contribution.

6. Conclusions

Based on petrographic and geochemical data, the rocks of the Querari Complex presented in this work have been subdivided into two distinct facies: the Panã-Panã and Matapi facies. These deformed granites are highly siliceous ($SiO_2 > 67$ wt.%) and high in total alkali ($K_2O + Na_2O > 7.7$ wt.%), have calc-alkaline signature with metaluminous (Panã-Panã Facies) and peraluminous (Matapi Facies) character. In general, the Panã-Panã and Matapi facies are characterized by high contents of large-ion lithophile elements (LILE) and low HFSE/LILE ratios. In addition to the geochemical distinctions, both facies present the same deformational pattern.

Considering the data collected in this work and their correlation with geochemical, isotopic, and geochronological data from the literature, it can be inferred that the protoliths of the Panã-Panã and Matapi facies have been created from distinct sources in a continental magmatic arc environment between 1.80 and 1.74 Ga. The Matapi Facies probably derived from partial melting of metasedimentary rocks, while the Panã-Panã Facies probably derived from partial melting of a meta-ignea source of intermediate composition, such as composition tonalitic gneisses. During its emplacement on the crust, $S_0//S_1$ foliation developed with NE-SW direction on Statherian. A second tectonic-metamorphic event, on amphibolite facies between 1.54 and 1.47 Ga, generated the S_2 foliation with E-W direction, and I- and S-type granites that outcrop on the whole Rio Negro Province. The third event is associated with the intracontinental reworking of K´Mudku that ended up with the development of the S_3 foliation, with NE-SW direction, parallel to the S1 foliation. Unlike what can be seen in all other domains of Rio Negro Province, the K´Mudku event reached high temperatures in the Uaupés Domain (upper amphibolite facies). However, late low-temperature greenschist facies deformation is also recognized in the Uaupés Domain, revealed by ductile-brittle structures that are probably related to the late stages of the K´Mudku event.

Considering that the same evolutionary pattern is attributed to both Cauaburi and Querari complexes, it is difficult to link their formation to distinct magmatic arcs (Cauaburi and Querari orogenies) as proposed by Almeida et al. (2013). Therefore, additional geochronological analyses are still needed to provide ages for each of the identified deformational events in the Querari and Cauaburi complexes to allow a further conclusion on this topic.

References

Almeida M.E. 1997. Petrografia e geoquímica de elementos maiores da Suíte Intrusiva Tiquié: o caso dos Granitos Tiquié e Marié-Mirim no Estado do Amazonas. In: Costa M.L., Angélica R.S. (coord.). Contribuições à Geologia da Amazônia. Belém, FINEP/SBG-NO, p. 22-45. Available on line at: http://arquivos.sbg-no.org.br/BASES/CGA%201.pdf / (accessed on 31 March 2021)

Almeida M.E., Macambira M.J.B., Scheller T. 1997. Içana Intrusive Suite: age 207Pb/206Pb (zircon evaporation) of muscovite-bearing granite, Amazonas State, Brazil. In: South-American Symposium on Isotope Geology, 4, 31-33.

Almeida M.E. 2006. Província Rio Negro. In: Reis N.J., Almeida M.E., Riker S.L., Ferreira A.L. (org.). Geologia e recursos minerais do Estado do Amazonas: texto explicativo dos mapas geológico e de recursos minerais do estado do Amazonas. Escala 1:1.000.000. Manaus, CPRM. p. 49-67. Available on line at: http://rigeo.cprm.gov.br/jspui/handle/doc/2967 / (accessed on 31 March 2021)

Almeida M.E., Macambira M.J.B., Santos J.O.S., Nascimento R.S.C., Paquette J.L. 2013. Evolução crustal do noroeste do Cráton Amazônico (Amazonas, Brasil) baseada em dados de campo, geoquímicos e geocronológicos. In: Simpósio de Geologia da Amazônia, 13, 201-204. Available on line at: http://arquivos.sbg-no.org.br/BASES/SGA%2013.pdf / (accessed on 05 April 2021).

Barker F., Arth J.G. 1976. Generation of trondhjemitic-tonalitic liquids and Archean bimodal trondhjemite-basalt suites. Geology, 4(10), 596-600. https://doi.org/10.1130/0091-7613(1976)4<596:GOTLAA>2.0.CO;2

Boynton W.V. 1984. Cosmochemistry of the rare earth elements: meteorite studies. In: Henderson P. (ed.) Rare Earth Elements Geochemistry, Developments in Geochemistry. Amsterdam, Elsevier, p. 63-114. https://doi.org/10.1016/B978-0-444-42148-7.50008-3

Carneiro M.C.R., Nascimento R.S.C., Almeida M.E., Salazar C.A., Trindade I.R., Rodrigues V.O., Passos M.S. 2017. The Cauaburi magmatic arc: Litho-stratigraphic review and evolution of the Imeri Domain, Rio Negro Province, Amazonian Craton. Journal of South American Earth Sciences, 77, 310-326. https://doi.org/10.1016/j.jsames.2017.06.001

Chappell B.W., White A.J.R. 1974. Two Contrasting Granite Types. Pacific Geology, 8, 173-174.

Chappell B.W., White A.J.R. 2001. Two contrasting granite types: 25 years later. Australian Journal of Earth Sciences, 48(4), 489-499. https://doi.org/10.1046/j.1440-0952.2001.00882.x

Cordani U.G., Sato K., Sproessner W., Fernandes F.S. 2016. U-Pb zircon ages of rocks from the Amazonas Territory of Colombia and their bearing on the tectonic history of the NW sector of the Amazonian Craton. Brazilian Journal of Geology, 46(Suppl. 1), 5-35. https://doi.org/10.1590/2317-4889201620150012

Cox K.G., Bell J.D., Pankhurst R.J. 1979. The interpretation of igneous rocks. London George Allen & Unwin, 450 p. https://doi.org/10.1007/978-94-017-3373-1

Eby G.N. 1992. Chemical subdivision of the A-type granitoids: Petrogenetic and tectonic implications. Geology, 20(7), 641-644. https://doi.org/10.1130/0091-7613(1992)020<0641:CSOTAT>2.3.CO;2

Gibbs A.K., Barron C.N. 1993. The Geology of the Guiana Shield. New York, Oxford University Press, 245 p.

Gower R.J.W., Simpson C. 1992. Phase boundary mobility in naturally deformed, high-grade quartzofeldspathic rocks: evidence for

diffusional creep. Journal of Structural Geology, 14(3), 301-313. https://doi.org/10.1016/0191-8141(92)90088-E

Harris N.B.W., Pearce J.A., Tindle A.G. 1986. Geochemical characteristics of collision-zone Magmatism. In: Coward M.P., Reis A.C. (eds.) Collision tectonics. Geological Society, London, Special Publications, 19, 67-81. https://doi.org/10.1144/GSL.SP.1986.019.01.04

Hofmann A.W. 1988. Chemical differentiation of the Earth: the relationship between mantle, continental crust, and oceanic crust. Earth and Planetary Science Letters, 90(3), 297-314. https://doi.org/10.1016/0012-821x(88)90132-x

Ibanez-Mejia M., Pullen A., Arenstein J., Gehrels G.E., Valley J., Ducea M.N., Mora A.R., Pecha M., Ruiz J. 2015. Unraveling crustal growth and reworking processes in complex zircons from orogenic lower-crust: The Proterozoic Putumayo Orogen of Amazonia. Precambrian Research, 267, 285-310. https://doi.org/10.1016/j.precamres.2015.06.014

Janoušek V., Farrow C.M., Erban V. 2006. Interpretation of whole-rock geochemical data in igneous geochemistry: introducing Geochemical Data Toolkit (GCDkit). Journal of Petrology, 47(6), 1255-1259. https://doi.org/10.1093/petrology/egl013

Janoušek V., Hanžl P., Svojtka M., Hora J.M., Kochergina Y.V.E., Gadas P., Holub F.V., Gerdes A., Verner K., Hrdličková K., Daly J.S., Buriánek D. 2020. Ultrapotassic magmatism in the heyday of the Variscan Orogeny: the story of the Třebíč Pluton, the largest durbachitic body in the Bohemian Massif. International Journal of Earth Sciences, 109, 1767-1810. https://doi.org/10.1007/s00531-020-01872-2

Jayananda M., Chardon D., Peucat J.J., Capdevila R. 2006. 2.61 Ga potassic granites and crustal reworking in the western Dharwar Craton, southern India: Tectonic, geochronologic and geochemical constraints. Precambrian Research, 150(1-2), 1-26. https://doi.org/10.1016/j.precamres.2006.05.004

Kemp A.I.S., Hawkesworth C.J., Foster G.L., Paterson B.A., Woodhead J.D., Hergt J.M., Gray C.M., Whitehouse M.J. 2007. Magmatic and crustal differentiation history of granitic rocks from Hf-O isotopes in zircon. Science, 315(5814), 980-983. https://doi.org/10.1126/science.1136154

Kruhl J.H. 1996. Prism- and basal-plane parallel subgrain boundaries in quartz: a microstructural geothermobarometer. Journal of Metamorphic Geology, 14(5), 581-589. https://doi.org/10.1046/j.1525-1314.1996.00413.x

Laurent O., Martin H., Moyen J.F., Doucelance R. 2014. The diversity and evolution of late-Archean granitoids: evidence for the onset of 'modern-style' plate tectonics between 3.0 and 2.5 Ga. Lithos, 205, 208-235. https://doi.org/10.1016/j.lithos.2014.06.012

Li C., Yang W., Zhu L., Yang Z., Lin L., Su X., Zhang H. 2019. Petrogenesis, geochemistry and geological significance of Paleocene Granite in South Gangdese, Tibet. Acta Geochimica, 38, 883-896. https://doi.org/10.1007/s11631-019-00375-5

Liégeois J.P., Navez J., Hertogen J., Black R. 1998. Contrasting origin of post-collisional high-K calc-alkaline and shoshonitic versus alkaline and peralkaline granitoids. The use of sliding normalization. Lithos, 45(1-4), 1-28. https://doi.org/10.1016/S0024-4937(98)00023-1

Maniar P.D., Piccoli P.M. 1989. Tectonic discrimination of granitoids. GSA Bulletin, 101(5), 635-643. https://doi.org/10.1130/0016-7606(1989)101<0635:TDOG>2.3.CO;2

Manya S., Maboko M.A.H. 2016. Generation of Palaeoproterozoic tonalites and associated high-K granites in southwestern Tanzania by partial melting of underplated mafic crust in an intracontinental setting: constraints from geochemical and isotopic data. Lithos, 260, 120-133. https://doi.org/10.1016/j.lithos.2016.05.011

Mendes T.A.A., Mesquita R.B., Knauer L.G., Almeida M.E., Roncato J. 2020. Spatiotemporal constraints on the western Cauaburi Belt tectonics – northwestern Amazon Craton, Brazil. International Geology Review. https://doi.org/10.1080/00206814.2020.1768441

Miyashiro A. 1978. Nature of alkali volcanic rock series. Contributions to Mineralogy and Petrology, 66, 91-104. https://doi.org/10.1007/BF00376089

Patiño Douce A.E. 1999. What do experiments tell us about the relative contributions of crust and mantle to the origin of granitic magmas? In: Castro A., Fernandez C., Vigneresse J.L. (eds.) Understanding granites: Integrating New and Classical Techniques. Geological Society, London, Special Publication, 168, 55-75. https://doi.org/10.1144/GSL.SP.1999.168.01.05

Pitcher W.S. 1997. The nature and origin of granite. Springer, 403 p. https://doi.org/10.1007/978-94-011-5832-9

Priem H.N.A., Boelrijk N.A.I.M., Hebeda E.H., Verdurmen E.A.Th., Verschure R.H. 1971. Isotopic ages of the Trans-Amazonian acidic magmatism and the Nickerie Metamorphic Episode in the Precambrian basement of Surinam, South America. GSA Bulletin, 82(6), 1667-1680. https://doi.org/10.1130/0016-7606(1971)82[1667:IAOTTA]2.0.CO;2

Priem H.N.A., Andriessen P.A.M., Boelrijk N.A.I.M., Boorder H. de., Hebeda E.H., Huguett A., Verdurmen E.A.Th, Verschure R.H. 1982. Geochronology of the Precambrian in the Amazonas region of southeastern Colombia (western Guiana Shield). Geologie en Mijnbouw, 61(3), 229-242.

Santos J.O.S., Hartmann L.A., Gaudette H.E., Groves D.I., Mcnaughton N.J., Fletcher I.R. 2000. A New Understanding of the Provinces of the Amazon Craton Based on Integration of Field Mapping and U-Pb and Sm-Nd Geochronology. Gondwana Research, 3(4), 453-488. https://doi.org/10.1016/S1342-937X(05)70755-3

Santos J.O.S., Hartmann L.A., Faria M.S., Riker S.R., Souza M.M., Almeida M.E., McNaughton N.J. 2006. A compartimentação do Cráton Amazonas em Províncias: Avanços ocorridos no período 2002-2006. In: Simpósio de Geologia da Amazônia, 9, 156-159. Available on line at: http://arquivos.sbg-no.org.br/BASES/Anais%209%20Simp%20Geol%20Amaz%20Marco-2006-Belem.pdf / (accessed on 6 April 2021)

Santos J.O.S., Rizzotto G.J., Potter P.E., McNaughton N.J., Matos R.S., Hartmann L.A., Chemale Jr F., Quadros M.E.S. 2008. Age and autochthonous evolution of the Sunsás Orogen in West Amazon Craton based on mapping and U–Pb geochronology. Precambrian Research, 165(3-4), 120-152. https://doi.org/10.1016/j.precamres.2008.06.009

Schiano P., Monzier M., Eissen J.P., Martin H., Koga K.T. 2010. Simple mixing as the major control of the evolution of volcanic suites in the Ecuadorian Andes. Contributions to Mineralogy and Petrology, 160, 297-312. https://doi.org/10.1007/s00410-009-0478-2

Shand S.J. 1927. Eruptive Rocks: Their Genesis, Composition Classification and Their Reaction to Ore-Deposits. London, Thomas Murby and Co., 360 p.

Streckeisen A., Le Maitre R.W. 1979. A chemical approximation to the modal QAPF classification of igneous rocks. Neues Jahrbuch für Mineralogie, Abhandlungen, 136, 169-206.

Shang C.K., Liégeois J.P., Satir M., Frisch W., Nsifa E. N. 2010. Late Archaean high-K granite geochronology of the northern metacratonic margin of the Archaean Congo craton, Southern Cameroon: Evidence for Pb-loss due to non-metamorphic causes. Gondwana Research, 18(2-3), 337-355. https://doi.org/10.1016/j.gr.2010.02.008

Tassinari C.C.G., Cordani U.G., Nutman A.P., Van Schmus W.R., Bettencourt J.S., Taylor P.N. 1996. Geochronological Systematics on Basement Rocks from the Rio Negro-Juruena Province (Amazonian Craton) and Tectonic Implications. International Geology Review, 38(2), 161-175. https://doi.org/10.1080/00206819709465329

Thiéblemont D., Tégyey M. 1994. Une discrimination géochimique des roches différenciées témoin de la diversité d'origine et de situation tectonique des magmas calco-alcalins. Comptes Rendus de l'Académie Des Sciences. Série II, Sciences de la terre et des planètes, 319(1), 87-94.

Thompson R.N. 1982. Magmatism of the British tertiary volcanic province. Scottish Journal of Geology, 18(1), 49-107. https://doi.org/10.1144/sjg18010049

Tulibonywa T., Manya S., Torssander P., Maboko M.A.H. 2017. Geochemistry of the Palaeoproterozoic volcanic and associated potassic granitic rocks of the Ngualla area of the Ubendian Belt, SW Tanzania. Journal of African Earth Sciences, 129, 291-306. https://doi.org/10.1016/j.jafrearsci.2017.01.022

Veras R.S., Nascimento R.S.C., Almeida M.E. 2015. Litofácies Santa Isabel, embasamento do Domínio Içana, Província Rio Negro, Cráton Amazônico. In: Congresso Brasileiro de Geoquímica, 15. Available on line at: https://www.sbgq.org.br/anais-dos-congressos / (accessed on 6 April 2021)

Veras R.S., Nascimento R.S.C., Almeida M.E., Paquette J.L., Carneiro M.C.R. 2018. Paleoproterozoic basement of Içana Domain, Rio Negro Province, northwestern Amazonian Craton: geology, geochemistry and geochronology (U-Pb and Sm-Nd). Journal of South American Earth Sciences, 86, 384-409. https://doi.org/10.1016/j.jsames.2018.07.003

Wright J.B. 1969. A simple alkalinity ratio and its application to questions of non-orogenic granite genesis. Geological Magazine, 106(4), 370-384. https://doi.org/10.1017/S0016756800058222

Yund R.A., Tullis J. 1991. Compositional changes of minerals associated with dynamic recrystallization. Contributions to Mineralogy and Petrology, 108, 346-355. https://doi.org/10.1007/BF00285942